Uncertainty Quantification

of the lifetime of self-healing thermal barrier coatings based on surrogate modelling of thermal cyclic fracture and healing

Anuj Kumthekar

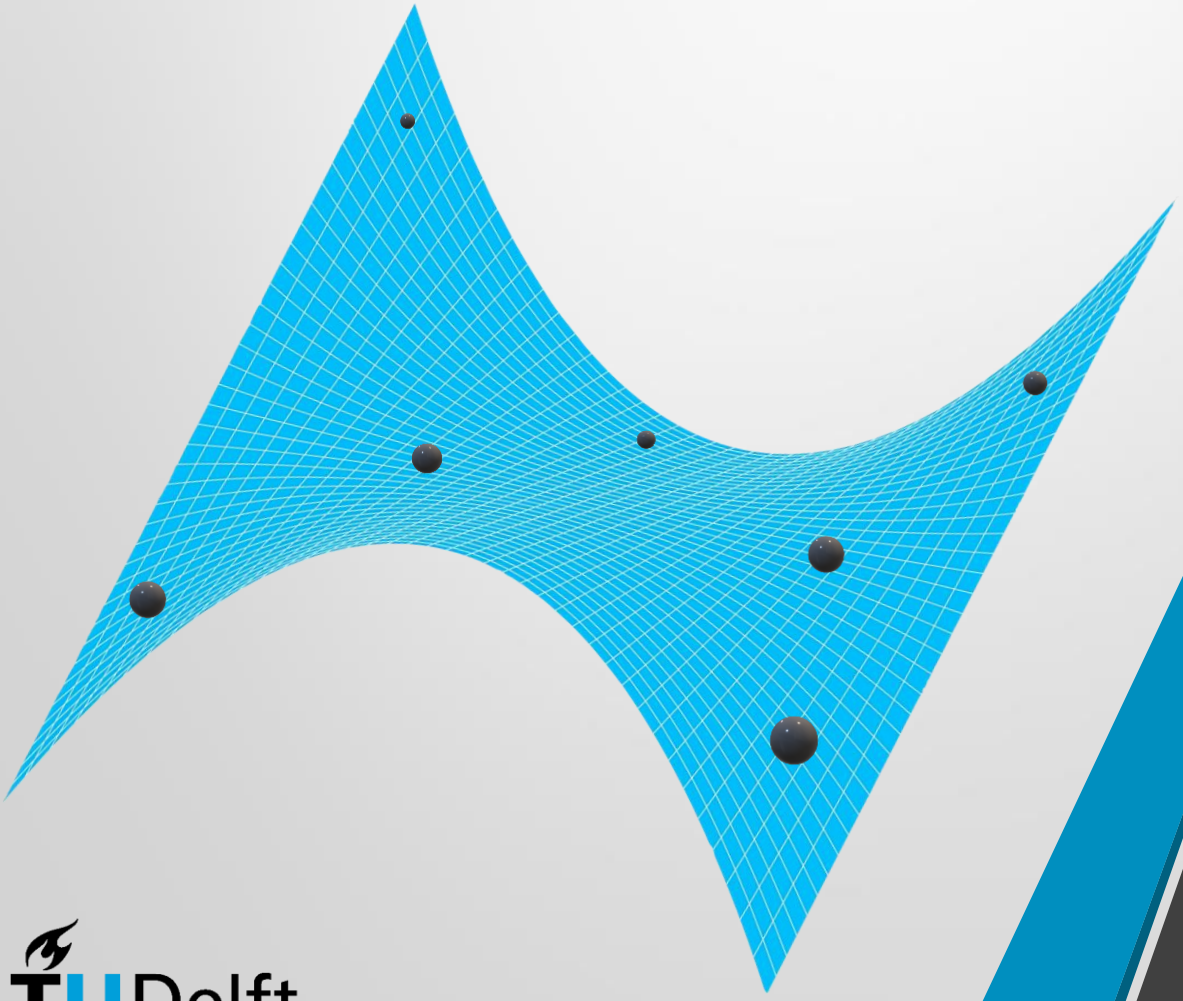

TU Delft

Uncertainty Quantification

of the lifetime of self-healing thermal barrier coatings based on surrogate modelling of thermal cyclic fracture and healing

MASTER OF SCIENCE THESIS

For obtaining the degree of Master of Science in Aerospace Engineering
at Delft University of Technology

Anuj Kumthekar

9 July 2021

Faculty of Aerospace Engineering · Delft University of Technology

DELFT UNIVERSITY OF TECHNOLOGY
FACULTY OF AEROSPACE ENGINEERING
DEPARTMENT OF AEROSPACE STRUCTURES AND MATERIALS

GRADUATION COMMITTEE

Date: 9 July 2021

Chair holder:

_____
Prof. Dr. Sybrand van der Zwaag

Committee members:

_____
Dr. Sergio Turteltaub

_____
Dr. Boyang Chen

_____
Dr. Sathiskumar A Ponnusami

ABSTRACT

Thermal barrier coatings (TBCs) are thermal insulation coatings which are utilized to protect the underlying substrate from high temperature degradation. They consist of a refractory ceramic top coat (TC) layer which is adhered to the substrate with the help of a metallic bond coat (BC) layer. Upon prolonged exposure to thermal cycling, stresses are developed within TBCs which lead to formation and growth of microcracks. Eventually, these cracks coalesce and lead to spallation of the TBC which exposes the underlying material to a temperature it cannot cope with. In order to arrest crack growth and increase the TBC lifetime or the number of thermal cycles until spallation, researchers have proposed the inclusion of self-healing particles within the TBC. Several finite element (FE) models have also been developed to study the impact of microstructural parameters on the TBC lifetime with the help of numerical simulations.

However, since the simulations are deterministic in nature, the FE methods are unable to take into consideration the uncertainties in the microstructural design variables and knowing how to cope with such uncertainties provides a scope for improving the reliability of simulation outputs. In order to consider the uncertainties in input variables, a brute force approach such as Monte Carlo simulation (MCS) can be utilized in which random sampling of the input variable distribution is carried out using which the finite element simulations can be run. However, since each simulation is computationally expensive, MCS tends to be inefficient. In order to circumvent this, a surrogate model can be utilized which is calibrated based on a limited number of runs of the underlying model and is able to emulate the original model in a computationally inexpensive manner.

In this thesis, a 2D micromechanical model for a TBC containing discrete healing particles with a known healing response is considered whose response to thermal cyclic behaviour has been described using a cohesive-zone based crack healing model. Variables such as the TC/BC interface amplitude, growth rate of thermally grown oxide layer at the TC/BC interface, diameter and volume fraction of healing particles, and the mean distance of particles from the TC/BC interface have been used to design the TBC FE model. A polynomial chaos expansion based surrogate model is developed which considers uncertainties in the design variables as inputs and the TBC lifetime as the output. The trained surrogate model has been used to obtain the statistical characteristics of the TBC lifetime as well as the sensitivity indices of the input variables.

The TC/BC interface amplitude has been found to be the most significant contributor to variance in the TBC lifetime, with the parameters describing the healing particles topology displaying a relatively minor influence. An additional model has been developed which acts as a surrogate to the TBC micromechanical model without any healing particles. A comparison of the realizations of TBC lifetimes generated using the two developed surrogate models indicates that the implementation of self-healing particles within the TBC domain increases the expected value of TBC lifetime, however, it also leads to an increase in the scatter of thermal fatigue life as compared with the benchmark case or the TBC model without healing particles. The thesis also contains a side study on the optimal number of processors to be used in parallel to minimize the total computing time.

ACKNOWLEDGEMENTS

I consider myself to be really fortunate to have carried out this research under the supervision of Dr. Sybrand van der Zwaag and Dr. Sergio Turteltaub. I am grateful to them for giving me the opportunity to work on such an intriguing and novel thesis topic. I would like to thank them for taking out time from their busy schedules and providing me with timely feedback. Their sustained enthusiasm combined with a strong attention to detail promoted insightful discussions between us which kept me motivated throughout the duration of my thesis.

I would like to express my thanks to Dr. Jayaprakash Krishnasamy whose advice and guidance in the beginning helped me to have a smooth start to the project. I would also like to thank Gawel Kus for suggesting me helpful resources to improve my understanding of the supporting research topics. My sincere thanks to all the colleagues at NovAM! Although I could not spend much time with them in person, I really appreciate the online group meetings which helped develop a sense of belonging in addition to being helpful by providing important tips on carrying out research.

I would also like to thank all the friends at TU Delft, who helped me make countless memories, right from the introduction programme till the end of the Master's period. Special thanks to Nikhil, Siddharth, Krishna, Mark and Caspar for keeping me company and for never failing to cheer me up!

Finally, there are no words to describe how grateful I am to my parents and family members who have been a source of constant motivation and encouragement. I would like to thank them for always being supportive in my decisions and for their unwavering care without which this thesis would not have been possible.

Anuj Kumthekar
Delft, July 2021

TABLE OF CONTENTS

LIST OF FIGURES

LIST OF TABLES

1

INTRODUCTION

In this introductory chapter, a brief overview of thermal barrier coatings is presented along with the processing methods and the resulting microstructure. This is followed by a description of potential causes of failure and the concepts behind self-healing thermal barrier coatings. Towards the end of the chapter, an outline of the different micromechanical modelling techniques as well as the concept of metamodeling are described. The chapter ends with a brief description of the thesis structure.

1.1. THERMAL BARRIER COATINGS

Thermal barrier coatings (TBCs) are thermal insulation coatings that are utilized in high temperature environments such as turbines, internal combustion engines and pyrochemical processes in order to protect the underlying structural substrate from thermal degradation and to improve the operating temperature range and thermodynamic efficiency [1]. In the aerospace industry, TBCs play a prominent role since it is the most commonly used process to protect jet turbine blades. Consequently, the safety and integrity of the turbines as well as maintenance and reparation schedules strongly depend on the lifetime of these systems.

A typical TBC is composed of a bond coat (BC) and a top coat (TC). The TC is a refractory layer made up of a ceramic material that should possess properties such as low thermal conductivity, high melting point and a coefficient of thermal expansion similar to that of the substrate [2]. It is usually made up of zirconia which is stabilized by 7-8wt % yttria [3] in order to prevent unwanted volumetric changes due to phase transformation at temperatures around 1150°C. The BC provides adhesion between the top coat and the metallic substrate as well as acts as a sacrificial layer which prevents the oxidation of underlying substrate. It is usually made up of Nickel-Chromium alloys such as NiCoCrAlY, NiCrAlY etc. At high operating temperatures, the diffusion of oxygen occurs within the TBC and it reacts with the aluminium component of the bond coat resulting in formation of a thermally grown oxide layer Al_2O_3 (TGO) at the interface of BC and TC [4].

One of the most important aspects that influence the performance of a TBC is its microstructure. The TBC microstructure depends on the manufacturing methods, some of which are atmospheric plasma spraying (APS), electron beam physical vapor deposition (EB-PVD), suspension plasma spraying (SPS), plasma spray physical vapor deposition (PS-PVD) and solution precursor plasma spraying (SPPS). APS and EB-PVD are the commonly used manufacturing methods. However, the latter are incorporated in order to further tailor TBC performance and durability by developing multi-layered and functionally graded structures [2]. APS is one of the thermal spraying techniques that is being preferably used in industries because of its operability in a wide range of process temperatures and also because it is comparatively cheaper than other techniques.

In APS, the ceramic powdered feedstock is passed through the plasma plume which helps in the transfer of thermal energy and momentum to the powder particles. These melted particles then strike the surface of the substrate and solidify to form lamellar structures referred to as splats. Over the period of deposition, these splats generate a structure resembling a brick-wall. However, during this rapid process it is possible that the droplets do not wet the substrate surface completely before solidifying, resulting in the formation of interlamellar pores [5]. The presence of these pores helps in the reduction of the inherent thermal conductivity of the TBC. In the case of EB-PVD, a columnar microstructure is developed in the normal direction to the substrate. These coatings consist of intercolumnar gaps which contribute towards the amount of porosity [6]. This vapour-based fabrication technique results in lower contamination within the TBC and a good surface finish.

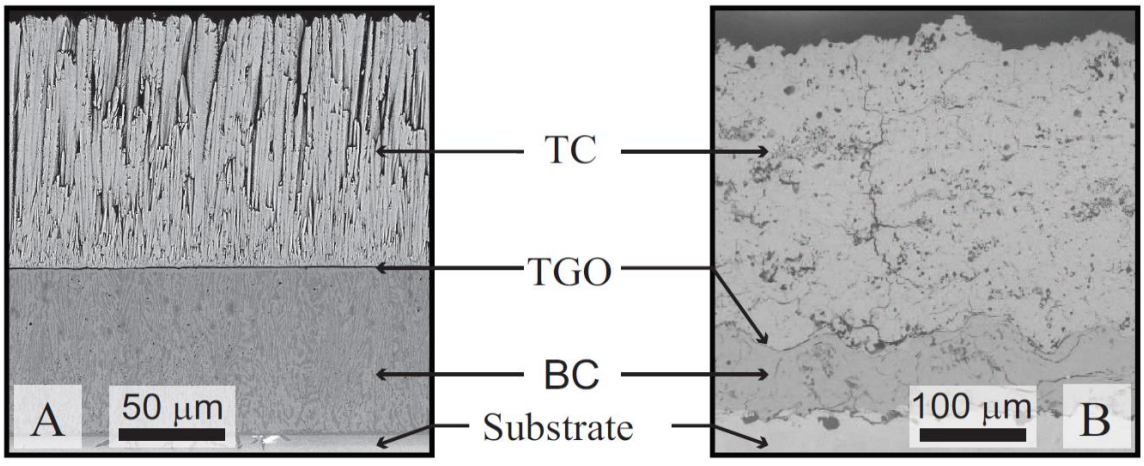

Figure 1.1: TBC micrographs generated by two deposition processes (a) EB-PVD (b) APS [7]

The columnar microstructure is also known to develop strain tolerant coatings due to the fact that there is lesser contact between different columns of the structure. This results in lower elastic modulus which helps to improve the thermal shock resistance. Figure 1.1 indicates the microstructural differences in the TBC system generated due to the different deposition processes. These different microstructures affect the response of the TBC to the external environment and hence the failure mechanisms. In case of the APS manufactured TBCs, the final failure is considered to have occurred when spallation occurs by the debonding of regions of the top coat from the bond coat. This exposes the area underneath the top coat to the harsh environment which may later lead to catastrophic failure. A special feature of APS produced TBCs is that due to the supersonic impact of TBC particles on the metallic substrate, the metallic component loses its smooth surface and a rough interface develops. The roughness of this interface has a strong effect on the lifetime [32]. The remainder of this thesis deals with APS produced TBCs, which is currently the most commonly used system in industry.

1.2. CAUSES OF FAILURE

Several factors leading to cracking and failure of TBCs have been identified by researchers and experimentalists such as residual stresses, mismatch of coefficient of thermal expansion (CTE) between the bond coat/substrate and the bond coat/top coat, thermal fatigue and formation of thermally grown oxide [1,8]. Residual stresses can be generated within the TBC during manufacturing when the hot melted feedstock comes in contact with comparatively cooler substrate or pre-existing splats.

Residual stresses can also be caused by the mismatch of CTE between the substrate and the coating. This may lead to compressive or tensile stresses within the coating depending on whether the CTE of the coating is lower or higher than that of the substrate. Compressive residual stresses are favourable for crack closure while tensile stresses may lead to loss of adhesion and delamination [9]. The formation of a thin TGO layer at the interface between the top and bond coats results in compressive stresses that can affect the local stress field. Residual stresses are generated within the TGO when the temperature drops during thermal cycling. The TGO growth also leads to thermal expansion mismatch between the top coat/TGO and TGO/bond coat. This mismatch can lead to formation of microcracks near the interface zones. Propagation and coalescence of these microcracks may lead to delamination and final failure [9].

Another important cause of failure in TBCs is the phenomenon of sintering at high temperatures (> 1200°C). Sintering leads to coalescence within the microstructural domain which reduces the porosity and thus increases the thermal conductivity of the coating, which may cause creep degradation at the inner layers. Sintering also causes stiffening of the coating which can lead to dissimilar contractions between the coating and the substrate which would eventually cause microcracks [10].

One of the other major contributors to failure in TBCs is the penetration of calcium-magnesium-alumino-silicate (CMAS) volcanic dust particles into the top coat. At high temperatures, these deposits melt and are able to infiltrate the top coat due to capillary effect [11]. During the cooling phase of the thermal cycle, these deposits solidify and hence affect the elastic modulus and the thermal conductivity of the coating. Also, there exists a difference in thermal expansion coefficients between the deposited CMAS and the top coat material which leads to differential response to thermal cycling and hence promotes formation of microcracks.

1.3. SELF-HEALING THERMAL BARRIER COATINGS

In order to improve the operating lifetime of TBCs, researchers have investigated the implementation of self-healing particles within the coatings [12-14]. One of the most widely studied methods of incorporating self-healing properties in a TBC is to include encapsulated healing agents within the top coat, which is the location where cracks typically appear in TBCs. Once activated by a growing microcrack, they initiate a chemical reaction which fills the crack and restores the mechanical integrity. Figure 1.2 illustrates the concept.

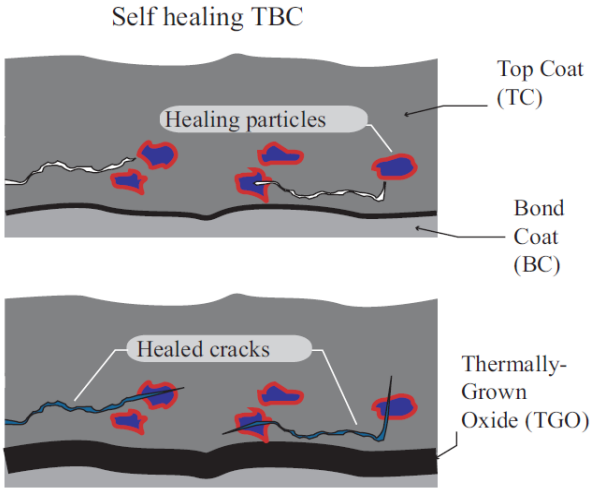

Figure 1.2: TBC healing mechanism in presence of cracks [15]

The high temperature stability requirement of the components necessitates that the healing agent should be solid yet still should be mobile enough to fill the generated cracks and inhibit further crack propagation [16]. The healing agent cannot be liquid due to higher CTE which would develop high strains during thermal cycling. After filling the crack, the healing agent should also be able to solidify through chemical reactions with the surrounding matrix material. One of the representative materials is molybdenum disilicide. When it reacts with oxygen, it forms molybdenum trioxide and silica which is indicated by the following reaction:

$$2MoSi_2\ (s) + 7O_2\ (g) \rightarrow 2MoO_3\ (g) + 4SiO_2\ (l)$$

Thus, when a crack encounters a healing particle, the above reaction will take place. From the reaction, it can be observed that for every mole of molybdenum disilicide, 2 moles of silica are produced which is indicative of volume expansion. At the usual turbine operating temperature, the silica is a viscous liquid which flows into the crack. Silica reacts with surrounding zircon (ZrO_2) and forms nanocrystalline zirconia ($ZrSiO_4$) and the molybdenum trioxide is emitted in gaseous form through the pores in the coating. Crack propagation is arrested due to the fact that the produced zirconate mechanically connects both crack faces and the material itself and is tougher than the YSZ top coat. The typical thickness values of the TC and BC are 500 µm and 200 µm respectively, whereas the self-healing particles possess a diameter ≈ 10 µm. It is preferred to deposit the healing particles near the TC/BC interface where cracking and delamination predominantly occur due to mismatch in thermomechanical properties of individual layers [13].

1.4. MODELLING THE FRACTURE BEHAVIOUR

Several techniques have been developed and implemented by researchers for simulation of crack propagation behaviour through the TBC domain and other similar heterogeneous media. Researchers have utilized techniques such as Cohesive Zone Modelling (CZM) [17-25], Extended Finite Element Method (XFEM) [26-32] and the Virtual Crack Closure Technique (VCCT) [33-35] for modelling and simulating the damage evolution. However, while using the VCCT, an initial crack needs to be specified and also the path of crack propagation needs to be defined before carrying out the simulation [36]. And in case of XFEM, it is difficult to simulate the penetration of two different cracks towards a single element [37] as well as the behaviour of cracks at an interface [36].

These difficulties can be overcome with the help of CZM and therefore this technique will be utilized in the project. Although CZM presents several advantages over the other numerical techniques, it results in computationally expensive simulations. For example, a cohesive zone element based finite element model consisting of ≈ 5 x 10^5 elements consumes a total of 40-50 CPU hours on a high performance computing cluster.

Also, finite element methods are deterministic as a result of which they are unable to take into consideration the uncertainties in microstructural variables used for developing the finite element model. Therefore, it becomes necessary to investigate the ways of quantifying uncertainties in the variables used for micromechanical simulations and understand whether the original finite element model can be substituted with a computationally inexpensive input-output relationship or a metamodel.

1.5. SURROGATE MODELLING

Surrogate modelling or metamodeling is a technique using which an approximate model of the original computational model is developed with the help of a limited number of runs of the original model [38]. The constructed surrogate model is computationally inexpensive and thus can be utilized for several number of runs which would not have been feasible for the original model. This could thus help in robust designing of input parameters. Commonly utilized surrogate models are Polynomial Chaos Expansion (PCE) and Gaussian Process (GP). Even though both the approaches are comparable in terms of performance and accuracy, PCE is preferred due to its ease of applicability and the underlying simplicity with which the relative contribution of input parameters to the output response can be obtained [38]. Surrogate modelling approaches have been applied by researchers in various fields involving complex and nonlinear model responses some of which include groundwater management [39, 40], sheet metal forming [41, 42], computational fluid dynamics [43, 44], design of composites [45, 46] and crack growth models [47, 48]. However, these metamodels which help in reducing computational expense have not yet been implemented for optimal designing of self-healing TBCs and modelling crack growth behaviour within the TBC domain.

Therefore, the thesis objective can be stated as follows: “To determine whether a surrogate modelling approach can be utilized to predict the lifetime of self-healing thermal barrier coatings by training a polynomial chaos expansion based metamodel with the help of limited number of runs of the cohesive zone based numerical model.” If a sufficiently reliable surrogate model can be generated, it might provide advantages such as strongly reduced computational expense in prediction of lifetime, determination of sensitivity to microstructural parameters, potential proposals to the manufacturing methods and hence robust designing of self-healing thermal barrier coatings.

1.6. THESIS ORGANIZATION

Chapter 2 introduces the relevant concepts of micromechanical modelling and the underlying cohesive zone modelling theory, presents the concept of uncertainty quantification and surrogate modelling along with a mathematical intuition behind polynomial chaos expansion and discusses the link between micromechanical modelling and quantification of uncertainty in input parameters. In Chapter 3, the computational framework for the thesis has been presented along with the implemented procedure. The results and validation of the trained surrogate model have been addressed in Chapter 4, along with a sensitivity analysis and the supporting discussion. The conclusion and recommendations for prospective research work are provided in Chapter 5.

2

THEORETICAL BACKGROUND

The proposed research brings together the fields of micromechanical modelling and metamodel-based uncertainty quantification. Section 2.1 introduces the concept of micromechanical modelling with a focus on the cohesive zone theory. Section 2.2 describes the idea of uncertainty quantification and surrogate modelling along with a mathematical intuition behind polynomial chaos expansion. Section 2.3 attempts to link these two different topics and provides the basic framework for the bridging and subsequent implementation. Finally, Section 2.4 indicates the prospective variables for development of the surrogate model, as proposed by the literature study.

2.1. INTRODUCTION TO MICROMECHANICAL MODELLING

A lot of research is being carried out in the field of micromechanical modelling of materials in order to understand the effects of heterogeneous microstructures in composite materials on the response to external stimuli. Basically, it involves the numerical modelling and analysis of certain controlled volumes of material. Micromechanical modelling approaches are generally classified into two categories: discrete and continuum models [49].

Discrete models are the ones in which a detailed simulation of the microstructural entities such as different geometries and phases is carried out. Some of the examples of this approach are particulate discrete element techniques, molecular dynamics and other numerical methods which are based on the requirement of detailed finite element analyses of particular heterogeneous features. As these models are computationally expensive and require extensive numerical efforts, the domain of study is restricted to small time and length scales.

On the other hand, continuum models consist of continuous distribution fields which are implemented along with constitutive relations and classical equations in order to obtain a modified continuum theory. In other words, these models are able to describe the general overall behaviour and do not focus on specific model heterogeneities.

One of the widely used methods for micromechanical numerical analysis is the utilization of a representative volume element (RVE) or a representative unit cell which consists of all the microstructural heterogeneous features in the material and is able to summarize the overall behaviour in terms of characteristics such as strength or fatigue life. The RVE is investigated with the help of finite element analyses by incorporating the required boundary conditions in order to understand its behaviour to applied stimuli and to project it to the overall material domain.

2.1.1 MODELLING THE TBC DOMAIN

The TBC domain consists of a complex microstructure which is made up of the bond coat layer, thermally grown oxide layer, top coat layer and also consists of features such as splats, pores and microparticles in case of self-healing thermal barrier coatings. The most common way of modelling the microstructure is with the help of a 2D representation in which the roughness of the TC/TGO layer is represented in either a sinusoidal form or a semi-circular form. This is because a 3D representation becomes computationally too expensive due to the microscale complexities [50]. The representative volume element is generally modelled with boundary conditions at either ends such as periodic boundary conditions [19, 24, 51] or symmetry boundary conditions [50,52]. Some of the other techniques of taking into account the intricacies of TBC domain are the use of random microstructure generation method [37] for development of arbitrary morphologies or the utilization of experimentally obtained SEM micrographs for post-processing and generation of finite element geometry [53].

2.1.2. THE COHESIVE ZONE METHOD

In accordance with the cohesive zone theory, cohesive elements are utilized in order to describe the crack propagation within the material. These are zero thickness elements which represent an interface and are indicative of the cohesive forces which occur when the material interfaces are being separated during crack growth. When damage occurs, these cohesive zone elements respond by opening and thus are able to simulate crack initiation and crack propagation. In finite element simulations, cohesive elements are implemented within the bulk material domain which is likely to be intersected by the simulated crack path. As a result, the direction of crack growth is dependent on the availability of the cohesive elements. These elements are in turn dependent on the amount of mesh refinement. A coarser mesh would imply a smaller number of cohesive elements while a finer mesh would indicate the presence of a greater number of cohesive elements. Thus, the material domain discretization should be fine enough such that the direction of crack growth does not vary much with change in mesh size [37].

The element failure behaviour is described with the help of traction-separation laws. Once a crack has been initiated, these laws describe the traction T across two crack surfaces as a function of the distance δ_n between them. Even though seemingly different forms of the traction-separation laws exist such as the bilinear, exponential, trapezoidal, polynomial forms, qualitatively they indicate a similar trend of traction variation. As the separation of the cohesive surfaces increases, the traction initially increases until a maximum value is reached, gradually starts to decrease and reaches zero when a threshold separation value δ_c has been attained. Figure 2.1 represents the mode I bilinear traction-separation law.

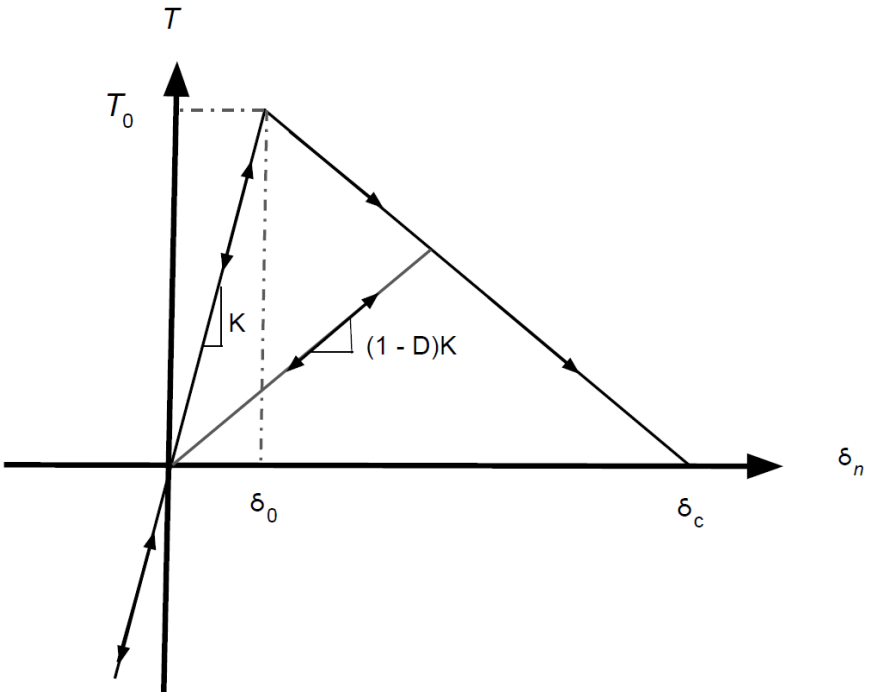

Figure 2.1: Bilinear cohesive traction-separation law

The initial slope of the traction-separation curve 'K' indicates the artificial penalty stiffness which is required to simulate a perfect bonding situation before onset of damage. 'D' represents the damage variable whose value lies between [0,1]. Its value for pure mode loading for a particular separation δ (where $\delta_0 \leq \delta \leq \delta_c$) can be evaluated as follows:

$$D = \frac{\delta_c(\delta - \delta_0)}{\delta(\delta_c - \delta_0)} \tag{2.1}$$

Thus, with the help of above relation, the stiffness degradation can be implemented when the separation between crack surfaces increases above δ_0. It can be observed that a relationship can be established between linear elastic fracture mechanics theory and the cohesive zone model with the help of the traction-separation law in which the area under the curve represents the fracture toughness G_c [37].

2.2. UNCERTAINTY QUANTIFICATION AND SURROGATE MODELLING

Computational models and numerical methods have been developed in order to establish relationships between structure, process and inherent structural properties which are difficult to be expressed analytically. These models are often deterministic, and hence from a given initial condition, will always produce the same response. As a result, it is assumed that there is no involved randomness in the formation of the output and that the parameters of the model can be deduced with absolute certainty. However, uncertainties in computer simulations can arise due to various reasons such as lack of complete information about the physical effects, incomplete parametrization of the model or having incomplete knowledge of the system state which is to be simulated [54]. These uncertainties can be classified into two groups: aleatoric and epistemic.

Aleatoric uncertainty is the one which results from inherent random variations in the quantity and thus cannot be reduced. It is generally managed by representing the variability in the form of probability distributions. For example, material microstructure and its resulting local behaviour can be associated with this type of uncertainty. Generally, in order to adequately quantify aleatoric uncertainty, identical instances of the studied system are extensively sampled. On the other hand, epistemic uncertainty is the one which arises from inaccurate or incomplete knowledge of the system which is being studied. As a result, it is reducible by gathering more information about the system parameters. Uncertainties arising from differing experimental conditions, human errors, calibration of measuring equipment or the methods of designing experimental procedure can be associated with epistemic uncertainties.

2.2.1. UNCERTAINTY QUANTIFICATION VS UNCERTAINTY PROPAGATION

Deterministic models consider only one of the several possible instances of the model parameters and hence ignore the effects of uncertainties on the response. Therefore, in order to support robust decision making, quantifying the model uncertainties and understanding how they affect the response by propagating them through the model is necessary. Once the uncertainties are identified or detected, they can be calibrated with the help of available data and represented in the form of probability distributions.

This calibration of the parameters is known as uncertainty quantification while the process of forward propagation of the uncertainties through the levels of the model in order to predict the response is known as uncertainty propagation. Uncertainty quantification and propagation can indicate the degree of robustness of the system by describing how the system responds to input variations, as indicated in Figure 2.2. This also helps in the design of parameters by presenting values of the input in such a way that their variations have a certain desired amount of effect on the output. Hence, uncertainty quantification can be regarded as an inverse process in which the variations in model parameters are determined by analysing the error between the mathematical model and some data which is available beforehand. As an output, the process of uncertainty quantification is able to provide a representation of the underlying parameters of the model in the form of multivariate probability distributions in which the covariance matrix indicates the correlations between the parameters.

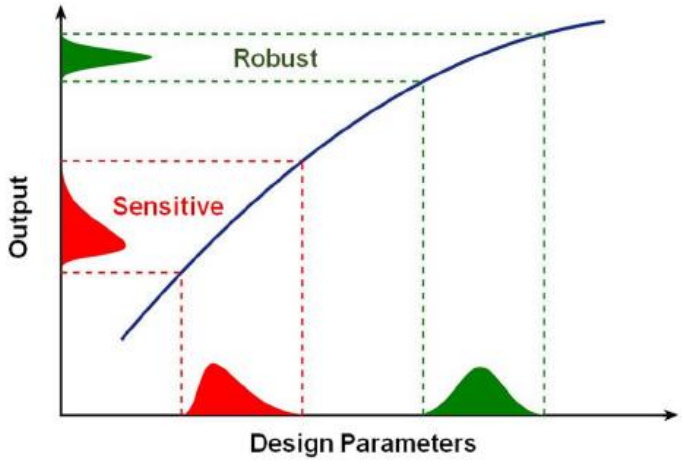

Figure 2.2: System output sensitivity with respect to input uncertainties [54]

Contrary to uncertainty quantification, the process of uncertainty propagation involves forward analysis in which the input uncertainties are mapped through the computational model in order to obtain the variations in the output. The most common method of carrying this out is by using Monte Carlo sampling which involves random sampling of input parameters and obtaining model outputs at these sampled points. However, models with high complexity render the MC sampling procedure impractical and computationally expensive. In order to reduce the computational effort, analytical techniques such as metamodeling or surrogate models have been proposed which are able to approximate the original model with functions which are easier to evaluate. Initially, a methodically chosen design of experiments (DOE) has to be carried out for generating support points for the surrogate model. The output values of the original model at these support points are obtained and then utilized to develop the response surface of the metamodel. As a result, the process of predicting the output values at points which were not considered in the DOE data collection scheme is simplified.

2.2.2. POLYNOMIAL CHAOS EXPANSION

Chaos represents the unpredictability and resulting disorder in complex systems as a result of lack of definitive information about the initial system conditions. Wiener [55] introduced the term 'homogeneous chaos' in which a Gaussian process representing a homogeneous dynamic system such as gas or liquid is characterized with the help of a generalized Fourier series expansion of Hermite polynomials. Polynomial chaos is a part of homogeneous chaos in which the states of the dynamic system were described with the help of polynomial representations. In accordance with the Cameron-Martin theorem [56], the homogeneous chaos converges to any processes which exhibit finite variance, as in the case of most physical processes. In other words, it becomes possible to represent a stochastic process with the help of a Fourier Hermite series expansion. A generalized Fourier series represents an expansion which is based on a set of orthogonal polynomials. A sequence of polynomials P_i, where i is a non-negative integer, is termed as orthogonal within the interval $[m, n]$ if it follows the following:

$$\int_m^n P_i(x)P_j(x)w(x)dx = h_i\delta_{ij} \tag{2.2}$$

Here, w represents the weight function, h_i are constants and δ_{ij} is the Kronecker delta

$$\delta_{ij} = 1 \quad if\ i = j$$

$$\delta_{ij} = 0 \quad if\ i \neq j$$

Different classes of polynomials have different weight functions with respect to which they are orthogonal within the specified interval. For example, the weight function in case of Hermite polynomials is $e^{-\frac{x^2}{2}}$, to which they are orthogonal within the limits $(-\infty, \infty)$. In agreement with the Cameron-Martin theorem, Xiu & Karniadakis [57] have demonstrated that a chaos expansion based on Hermite polynomials has an optimal convergence rate to the underlying stochastic process in case of a Gaussian process. Mathematically, this can be understood from the attribute that the form of the probability density function for Gaussian variables is same as that of the weight function for Hermite polynomials. They also observed that for processes involving distributions other than the Gaussian, the convergence rate is considerably slower.

Extending the work of Wiener's classical polynomial chaos, Xiu & Karniadakis introduced the idea of using family of polynomials known as the Askey scheme, that are orthogonal with respect to probability distributions following a non-Gaussian nature. The Askey scheme provides different classes of polynomials for different distributions of random variables. For instance, the Legendre polynomials are utilized in case of a uniform distribution, Jacobi polynomials in case of a beta distribution, etc. [58]. Table 2.1 provides a summary of orthogonal weight functions and polynomial classes for specific distributions of random variables [59].

Distribution	PDF	Polynomial class	Weight function	Interval
Gaussian	$\frac{1}{\sqrt{2\pi}}e^{-\frac{x^2}{2}}$	Hermite	$e^{-\frac{x^2}{2}}$	$(-\infty,\infty)$
Uniform	$\frac{1}{2}$	Legendre	1	$[-1,1]$
Beta	$\frac{(1-x)^{\gamma}(1-x)^{\delta}}{2^{\gamma+\delta+1}B(\gamma+1,\delta+1)}$	Jacobi	$(1-x)^{\gamma}(1-x)^{\delta}$	$[-1,1]$
Exponential	e^{-x}	Laguerre	e^{-x}	$[0,\infty)$

Table 2.1: Orthogonal polynomial classes for random variable types [59]

According to the classical polynomial chaos developed by Wiener, which is based on Hermite polynomials, a general second-order stochastic process can be represented in the following form [57]:

$$Y(x) = \alpha_0 H_0 + \sum_{i_1=1}^{\infty} \alpha_{i_1} H_1\left(\varphi_{i_1}(x)\right) + \sum_{i_1=1}^{\infty}\sum_{i_2=1}^{i_1} \alpha_{i_1 i_2} H_2\left(\varphi_{i_1}(x), \varphi_{i_2}(x)\right) + \cdots,$$

Here, H indicates the Hermite polynomials in terms of independent Gaussian input variables $(\varphi_{i_1}, \varphi_{i_2}, \ldots, \varphi_{i_n})$. The above-mentioned expansion can also be represented in the following form [60]:

$$Y = \sum_{i=0}^{\infty} y_i \psi_i(\varphi) \tag{2.3}$$

$\psi_i(\varphi)$ forms an orthogonal basis with respect to the joint probability density function of the input random variables and is obtained by carrying out a tensor product of the univariate orthogonal polynomials:

$$\psi_i(\varphi) = \prod_{j=1}^{k} P_j^{\alpha_j^i}(\varphi_j) \tag{2.4}$$

Here, α_j^i represents the order of the univariate orthogonal polynomial P_j. The above series expansion is often truncated to a polynomial of order n since the response of the system converges after a certain number of terms and consideration of additional terms does not make any notable contribution towards the system response [46]. Hence, it also follows that $0 \leq \sum_{j=1}^{k} \alpha_j^i \leq n$.

$$Y = \sum_{\alpha=0}^{Q-1} y_i \psi_i(\varphi) \tag{2.5}$$

$$Q = \frac{(k+n)!}{k!\,n!} \tag{2.6}$$

Thus, the polynomial expansion is reduced to Q number of terms which is a function of the number of input random variables k and the maximum order of the expansion n. Polynomial chaos expansion is used for surrogate modelling in which it aims to approximate the response of the original computationally expensive model. This can be done by calibrating the surrogate model with the help of responses from the original model at certain number of sampled points from the input vector space. This tendency of the surrogate model to fit the response from the underlying original model is dependent on the computation of the coefficients y_i. As an example, Table 2.2 summarizes the types of Hermite polynomials for different orders of PCE. Here, we shall consider $k = 2$ and $n = 3$, thus giving $Q = 10$ by using Equation (2.6).

i	PCE order	i^{th} Polynomial
0	$n = 0$	1
1	$n = 1$	ϕ_1
2		ϕ_2
3	$n = 2$	${\phi_1}^2 - 1$
4		${\phi_2}^2 - 1$
5		$\phi_1\phi_2$
6	$n = 3$	${\phi_1}^3 - 3\phi_1$
7		${\phi_2}^3 - 3\phi_2$
8		$\phi_1({\phi_2}^2 - 1)$
9		$\phi_2({\phi_1}^2 - 1)$

Table 2.2: Types of 2D Hermite polynomials

Figure 2.3 gives an idea about how the order of PCE affects the shapes of polynomial bases which are used to approximate the underlying model for the case of two dimensional Hermite polynomials. It can also be observed that a polynomial expansion generated with the help of these basis functions is ideal for continuous functions in the considered variable distribution domain but may not handle thresholds or abrupt changes too well.

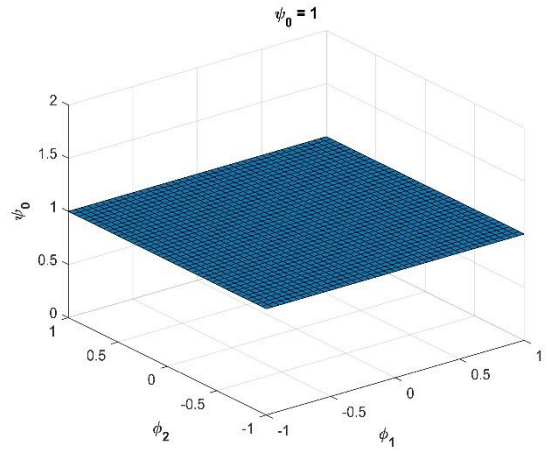
$\psi_0 = 1$
ψ_0
ϕ_1
ϕ_2

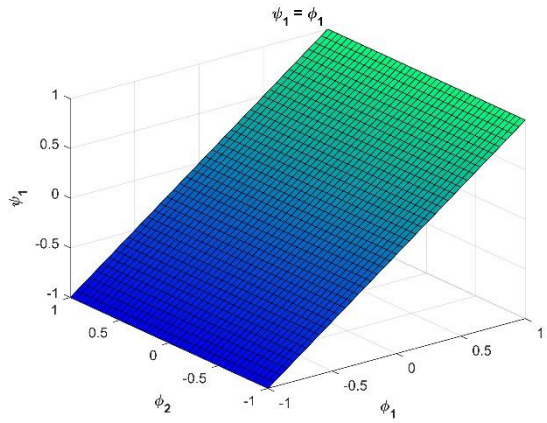
$\psi_1 = \phi_1$
ψ_1
ϕ_1
ϕ_2

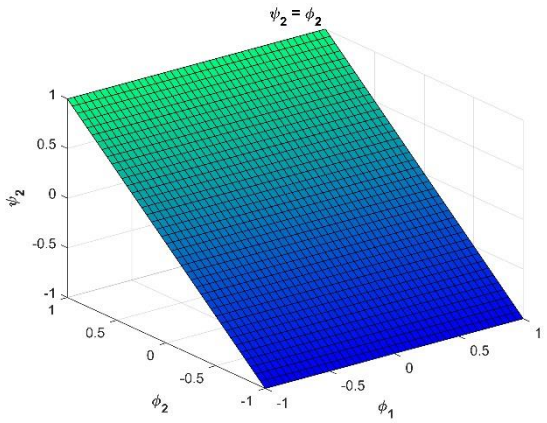
$\psi_2 = \phi_2$
ψ_2
ϕ_1
ϕ_2

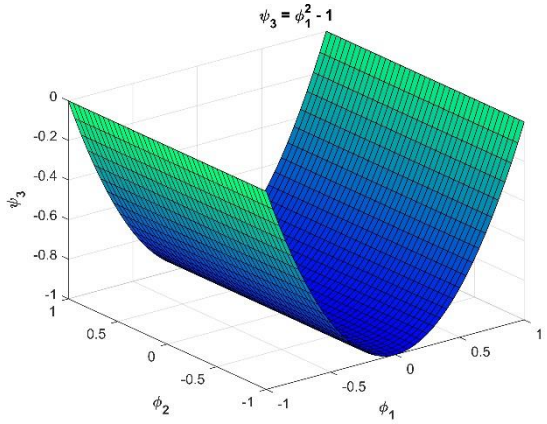
$\psi_3 = \phi_1^2 - 1$
ψ_3
ϕ_1
ϕ_2

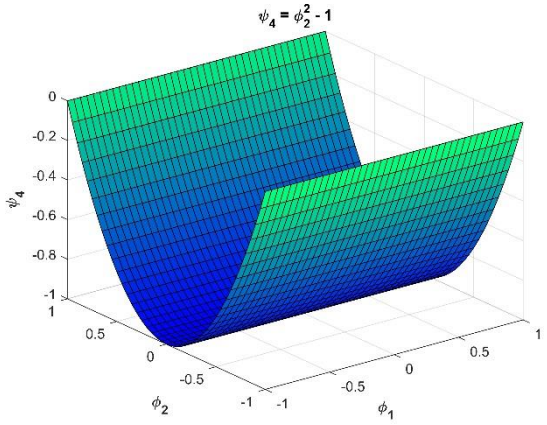
$\psi_4 = \phi_2^2 - 1$
ψ_4
ϕ_1
ϕ_2

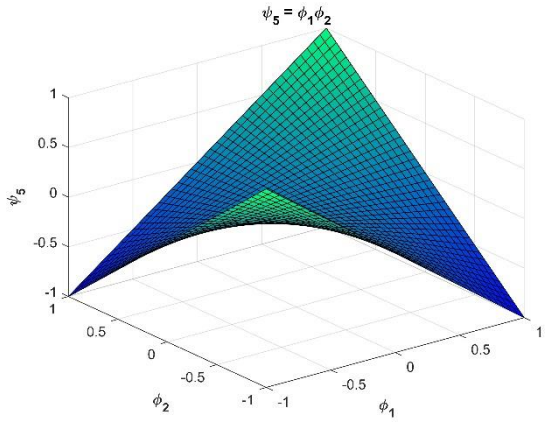
$\psi_5 = \phi_1\phi_2$
ψ_5
ϕ_1
ϕ_2

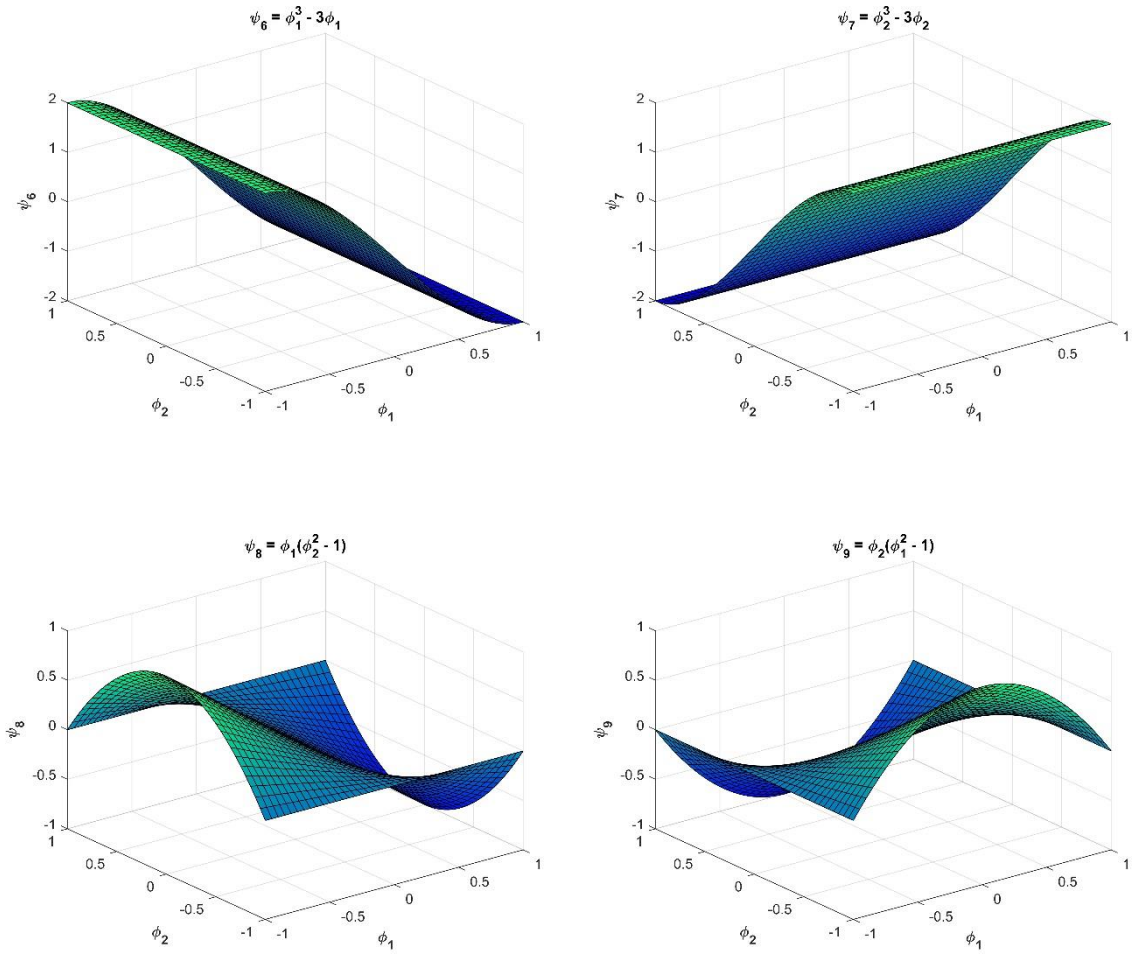

Figure 2.3: Set of 2D Hermite polynomials for PCE order = 3

Generally, the techniques used to compute the coefficients are divided into two classes: intrusive and non-intrusive methods. As the name suggests, intrusive methods involve modification of the original finite element code in which residual minimization has to be carried out in the weak form of the mathematical model or the utilization of the Galerkin approach. This weak form can be generated by projecting the original model on the polynomial chaos basis function [61]. On the other hand, the non-intrusive methods do not require alteration in the original deterministic finite element code. One of the widely used non-intrusive techniques is the least squares approximation or the point collocation approach. Once the sampling of input vector space is carried out, the sum of squares of residuals between the output of the exact model and the approximated PCE model solution is calculated [45].

$$S = \sum_{t=1}^{N} \left(Y_t(\varphi_t) - \sum_{i=0}^{Q-1} y_i \psi_i(\varphi_t) \right)^2 \tag{2.7}$$

Equating the partial derivative of the above equation with respect to each of the coefficients to zero and solving the resulting system of linear equations provides the required coefficients.

$$\frac{\partial S}{\partial y_i} = 0;\ i = 0,1, \dots, Q-1 \tag{2.8}$$

2.2.3. SAMPLING STRATEGIES

In order to train the PCE surrogate model, the original model needs to be evaluated at certain number of sampled points from the design space of the input variables. Thus, it requires a design of experiments for the generation of the trained data set [62]. Several experimental design methods have been developed by researchers over the years which have been utilized in order to obtain surrogate models for computer simulations. One of the earlier developed sampling techniques is the 2k factorial design methodology. It is based on the "one factor at a time" approach in which one of the input variables is varied while keeping the others fixed and then observing the variation of the system response [63]. This process is then repeated for all the variables in order to obtain the sensitivity of output response to each of the input variables. As a result, this leads to high computational effort due to the requirement of large number of simulations.

Another popular sampling strategy is the Monte Carlo sampling in which a sample value for an input variable is randomly chosen while adhering to the probability distribution of the input variable. Even though it has been known to be a robust experimental design approach, Monte Carlo sampling is inefficient in practical terms due to the requirement of large sample sizes for achieving space-filling characteristics within the input variable design space [62]. Additionally, if the sample sizes are not large enough, it is often observed that sample points are close to each other and this clustering can lead to inaccuracies in approximation of the original model. Quasi Monte Carlo sampling (QMCS) is an improvement over the traditional Monte Carlo sampling (MCS) approach in which clustering of samples is avoided, thus ensuring more uniformity of sample distribution within the design space. This technique is also known to exhibit better convergence rate than that of MCS. However, it is generally known to be best applied in case of uniformly distributed input variables [62].

Latin Hypercube sampling is an experimental design approach which is known to circumvent the issues exhibited by previously mentioned methods. It is inspired by the work of the mathematician Leonhard Euler who developed the concept of the Latin Square while working in the field of combinatorics. A Latin square consists of an $m \times m$ matrix which is filled with m different entities. They are filled in a way such that each entity is present only once in each row and each column [64]. This can be visualized in the example mentioned in Figure 2.4. Similarly, Latin Hypercube sampling (LHS) consists of dividing the input variable space into different levels and then choosing a representative value from each of the levels such that the selected value occurs exactly once in each dimension. Thus, this method is also known as the stratified sampling approach. LHS has been known to demonstrate the requirement of a smaller number of sampled points for covering the design space as compared with other sampling techniques. Dutta & Gandomi [62] have compared the error estimates of a surrogate model developed using different sampling schemes and have demonstrated that LHS possesses more desirable values for error in approximating the original model than that of MCS and QMCS.

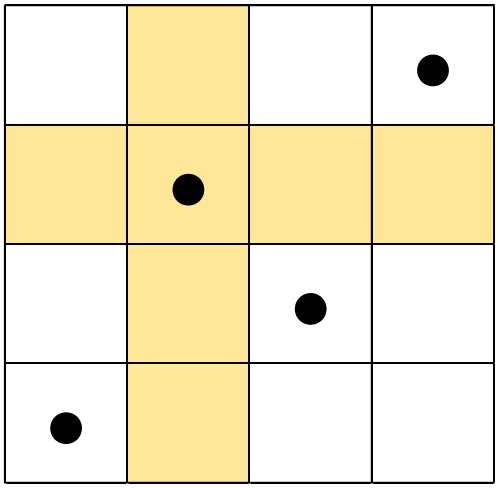

Figure 2.4: Latin square with four samples

Using LHS, it can be ensured that all sections within the ranges of input parameters are represented while being computationally efficient [65]. The following steps summarize the application of LHS to multivariate distributions [66]:

1. Divide the probability density function of each input variable into N non-overlapping equiprobable intervals.
2. Randomly sample one value from each interval.
3. Repeat steps 1 and 2 for all input variables.
4. Randomly pair the N values acquired for each variable with the values obtained for other variables.

These sampled points can be used to train the surrogate model in order to obtain the polynomial coefficients using least square approximation. However, it can be intuitively understood that the number of points to be sampled will affect the accuracy and variance of the surrogate model since these are the points at which the surrogate model will fit to the underlying original model. Hosder et al. [67] studied the influence of number of sampled points on the accuracy of the PCE. According to Equation (2.6), the number of coefficients Q to be evaluated in the PCE model depend on the number of input random variables k and the maximum order of the expansion n. Hosder et al. related the number of PCE coefficients with the number of points to be sampled with a parameter known as the oversampling ratio n_p [68] and suggested that a better approximation at each polynomial order can be obtained for $n_p = 2$.

$$n_p = \frac{number\ of\ sampled\ points}{Q} \tag{2.9}$$

2.3. LINKING UNCERTAINTY QUANTIFICATION AND MICROMECHANICAL MODELLING

Researchers have developed different numerical models in order to study the impact of microstructural variables on crack growth behaviour in TBCs. However, in the numerical analyses, the values for the variables have been kept unchanged for a particular set of parametric simulations while the exact values and variations are not known. As a result, the uncertainties within those parameters are not propagated through the finite element model and thus the reliability of the model output cannot be definitively stated. In order to take these uncertainties into account and provide a degree of confidence in the model outputs, various uncertainty quantification and surrogate modelling techniques are being employed.

The basic procedure utilized to develop a framework for uncertainty quantification is described in Figure 2.5. When surrogate modelling techniques are to be used in conjunction with finite element models, the initial step is to obtain a mapping between the input system variables and the computational model output. This relation is described with the help of a black box model in which only the input-output correlation is considered and not the actual intricacies of the associated function. This is indicated by the Step A in the figure. This is followed by the definition of a stochastic model of the input variables with the help of available information and expert understanding, as indicated by Step B. The individual stochastic descriptions are used to generate a joint probability density function of the input parameters. Then in Step C, the uncertainties in the input variables are propagated through the underlying model in order to obtain the response of interest which is treated as a random variable.

Properties of the response such as its mean and standard deviation can be useful for analysis and the determination of model output reliability. For example, in micromechanical modelling of thermal barrier coatings, the response of interest could be the final crack size whereas the input parameters could be the TGO growth rate, interface waviness as well as the strength of the top coat. This is then followed by Step C' in which sensitivity analyses can be carried out in order to determine the relative contribution of input parameters towards the variation in the output. As a result, the less contributing factors can be identified and then considered to be deterministic in order to reduce the computational effort.

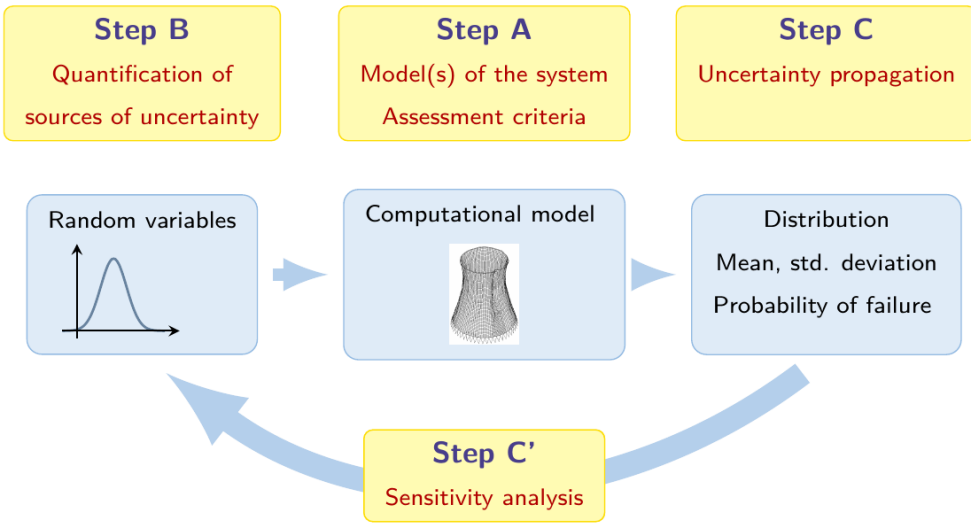

Figure 2.5: General framework for uncertainty quantification [69]

2.4. VARIABLES FOR POLYNOMIAL CHAOS EXPANSION

The APS technique, which is to be taken as the production method to create the self-healing TBCs to be analysed in this thesis, involves a feedstock powder which is fed into the plasma jet, as a result of which it melts and gets deposited on the substrate. Several parameters exist that influence the interplay between the plasma jet, the particles and the substrate. As a result, they influence the structure and properties of the deposited coating. Some of these parameters are the flow rate of plasma, amount of input energy, feedstock composition, particle size, powder injection distance, substrate temperature, powder fraction etc. [70].

Researchers have attempted to investigate the dependence of lifetime and failure of TBCs on its microstructure which is in turn dependent on the method of manufacturing and the processing parameters. However, due to the complexity of the manufacturing method and process variables, it is difficult to accurately predict the relations between not only the process and the microstructure but also the microstructure and properties of TBCs. More insights on these relations will help in better characterization, designing and prediction of reliability of TBCs. As a result, there exist uncertainties in the variables of the generated microstructure which need to be quantified in order to determine their influence on TBC durability and lifetime. We will now present the microstructural parameters experimentally or computationally known to have an effect on the TBC lifetime for conventional and self-healing TBCs.

2.4.1. INTERFACE AMPLITUDE

Researchers have studied the effects of top coat – bond coat interface geometry on the stress distribution and crack growth behaviour within the TBC as well as on its lifetime with the help of experiments and finite element simulations [71-73]. Eriksson et al. found that the amplitude of the interface depends on the size of the powder particles used as feedstock in the APS [71]. Therefore, an unpredictability in the size of powder particles could lead to an uncertainty in the value of the amplitude. They also observed that the roughness parameter attributed to the amplitude had a linear correlation with the TBC life. It was found that a ~50% change in the amplitude value led to a ~70% change in TBC life. On the other hand, they also observed that the equivalent wavelength of the interface profile was not correlated with the TBC life.

2.4.2. GROWTH RATE OF THERMALLY GROWN OXIDE LAYER

Another potential source of uncertainty in the prediction of TBC durability is the growth rate of thermally grown oxide (TGO) layer at the top coat – bond coat interface. Investigations carried out by researchers have indicated how the TGO layer thickness influences the stress redistribution and damage evolution within TBCs [74-77]. The growth of TGO layer occurs via the diffusion of oxygen ions through the ceramic top coat towards the TC/BC interface. It is difficult to accurately determine the oxygen flux since it depends on a number of parameters such as the stress levels, chemistry and microstructure of the TBC, which also depend on the spraying conditions during manufacturing [78]. Analysing the oxidation rates for a range of commercial super alloy compositions, deposition conditions and processes, Lim & Meguid have reconstructed the experimental upper and lower bounds for TGO growth rate at a dwell temperature of 1100°C [74], as indicated in Figure 2.6(a).

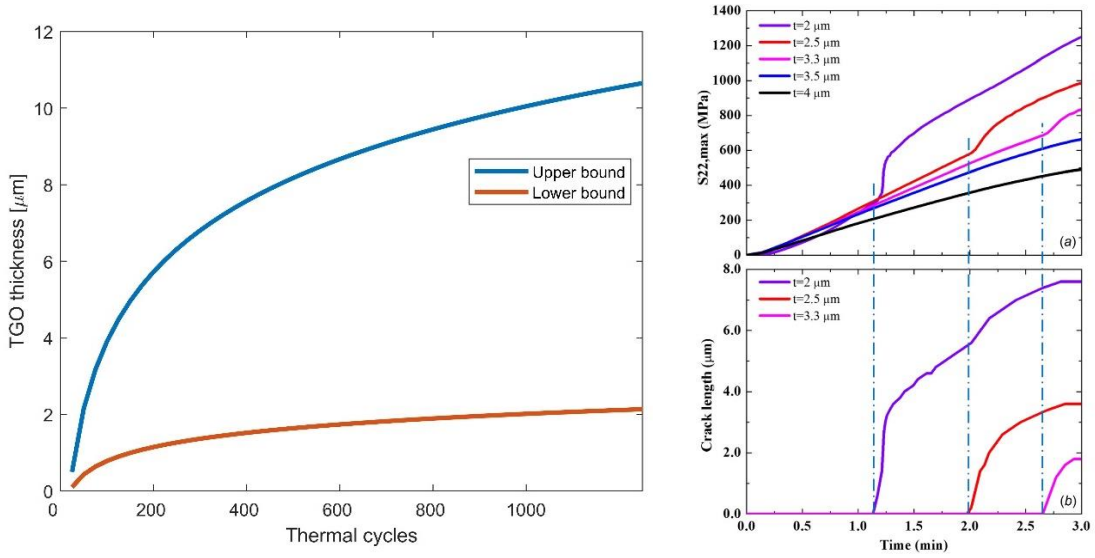

Figure 2.6(a) TGO growth with thermal cycles at dwell temperature = 1100°C [74], (b) variation of vertical normal stress and crack length for different TGO thicknesses during cooling [73]

Figure 2.6(b) describes the influence of varying TGO thicknesses on vertical normal stress in the top coat and crack length during cooling period. It has also been demonstrated by Ogawa & Nakano [79] that the quality of the TGO is also affected by the bond coating process. They observed that the TGO growth rate is lower when the bond coat is cold-sprayed whereas it is higher when the bond coat is sprayed using the low-pressure plasma spraying. Due to the complex interplay between stress levels, TGO thicknesses and diffusion rates of oxygen through the top coat, it becomes necessary to determine the sensitivity of stress distributions and crack growth behaviour to uncertainty in TGO growth rates in order to design coating lifetimes with allowable levels of variations in response to thermal cycling.

2.4.3. VOLUME FRACTION AND DIAMETER OF HEALING PARTICLES

In order to extend the lifetime of TBCs and also to reduce the rate of maintenance of components, researchers have proposed the incorporation of $MoSi_2$ healing particles in TBCs. However, implementing these healing particles in TBCs via APS, which is the most commonly used TBC manufacturing method, becomes difficult due to the more severe processing conditions involved. Also, there is a difference in melting points of the ceramic feedstock and healing particles which poses difficulties in achieving the desired TBC configuration. Koch et al. [83] have described an approach of manufacturing self-healing TBCs via APS by adjusting some of the underlying processing parameters. They have shown that by injecting healing particles at a certain offset from the point of injection of ceramic feedstock into the plasma jet, it becomes possible to deposit both components homogeneously.

This is because the plasma plume loses some of its energy while melting the ceramic feedstock and as a result, the plasma temperature reduces before it encounters the healing particles. However, despite being able to achieve a homogeneous distribution of healing particles within the TBC, the researchers found that the final configuration consisted of a reduced volume content of healing particles than desired (12% instead of the desired 20%). This can be attributed to the complexities in controlling the processing conditions such as variations in plasma jet temperature and velocity, differences in healing particle size, turbulence, mass flow rate of plasma, etc. While the technology to accurately control the particle volume fraction, particle size and average distance of particles from the TC/BC interface does not exist yet, the influence of healing particles on TBC behaviour in response to thermal cycling has been experimentally studied using spark plasma sintering process [80-82] and with the help of micromechanical simulations [14, 53].

For a given region or a layer near the TC/BC interface for distribution of healing particles, the volume fraction and size of healing particles determine the number of healing sites and amount of healing material available for recovering damage due to cracks within the TBC. This necessitates the prediction of the degree of influence which the variations in the healing particle volume fraction and particle size have on the TBC response to thermal fatigue. Such a study has not yet been carried out in the context of self-healing TBCs. However, in another investigation related to self-healing composites, the research carried out by Lv & Chen involves the study of self-healing efficiency of unhydrated cement nuclei in cementitious matrix material [84]. They concluded that the volume fraction as well as the distribution of particle size of cement nuclei are key factors affecting the self-healing efficiency. It was observed that the rate of self-healing increases with increase in volume fraction of the cement nuclei.

2.4.4. MEAN PARTICLE DISTANCE FROM THE TOP COAT-BOND COAT INTERFACE

Several experimental and numerical studies [70-73, 85] indicate that the TBC life is strongly influenced by the stress fields close to the TC/BC interface, primarily due to the interface roughness, growth of TGO layer as well as the mismatch in thermomechanical properties between individual layers. Therefore, in order to achieve effective self-healing characteristics, it is necessary that healing particles lie close to the interfacial region which is prone to development of cracks and crack growth by coalescence. Research has also indicated that inclusion of healing particles within TBCs affects the fracture patterns as compared with that of a conventional TBC without healing particles [19]. Therefore, in order to predict the response to these complexities, it is necessary to understand the TBC crack growth behaviour and its lifetime as a function of uncertainty in mean particle distance from TC/BC interface which can occur as a result of lack of clarity regarding the above-mentioned processing parameters. The cracking and healing response of self-healing TBCs has been described in more detail in Chapter 3.

3

COMPUTATIONAL METHODOLOGY

This chapter describes the overall computational framework adopted in the project along with the implemented procedure. The approach is mainly divided into two parts: (a) obtaining the lifetime of self-healing thermal barrier coatings in response to thermal cycling and (b) using the obtained lifetime results as data points for training the surrogate model. A workflow summarizing the general computational strategy has been provided at the end of the chapter.

3.1. EVALUATION OF SELF-HEALING TBC LIFETIME

3.1.1 TBC MICROMECHANICAL MODEL

The self-healing TBC micromechanical model developed by Krishnasamy et al. [14] has been utilized in order to obtain the number of cycles to TBC failure as a consequence of exposure to thermal cyclic behaviour. Figure 3.1 describes the representative element for the self-healing TBC micromechanical model. A two-dimensional framework has been utilized to model the unit cell under plane strain condition. It consists of the ceramic top coat (TC), metallic bond coat (BC), thermally grown oxide (TGO) layer at the TC/BC interface and self-healing particles. The roughness of the interface as well as the splat boundaries have been modelled in the form of sinusoidal curves. The influence of the substrate has been taken into account in the form of periodic boundary conditions for the displacement components d_x and d_y at the left (L) and right (R) edges of the unit cell,

$$d_x^R - d_x^L = (1 + \nu_{sub})\alpha_{sub}\Delta T w$$

$$d_y^R - d_y^L = 0$$

Here, ν_{sub} and α_{sub} represent the Poisson's ratio and the coefficient of thermal expansion values for the substrate, respectively. The width of the unit cell is indicated by w, whereas ΔT is the change in temperature responsible for generation of thermal stresses. The above boundary condition is based on the assumption of relatively higher thickness of the substrate

as compared with that of the TBC as a result of which the contraction or expansion of the substrate is imposed on the TBC. Representative values have been assigned to the geometrical features where t_{TC} = 500μm, t_{BC} = 200μm and t = 15μm indicate the thicknesses of the TC, BC and the splats respectively whereas the wavelength of the sinusoidal interface curve has been assigned the value of 60μm. The healing particles have been assumed to be distributed near the TC/BC interface within a layer of thickness t_{HL}= 150μm. The lengths of the splats have been set in such a way that the overall aspect ratio is representative of an APS-manufactured TBC [14,71,86].

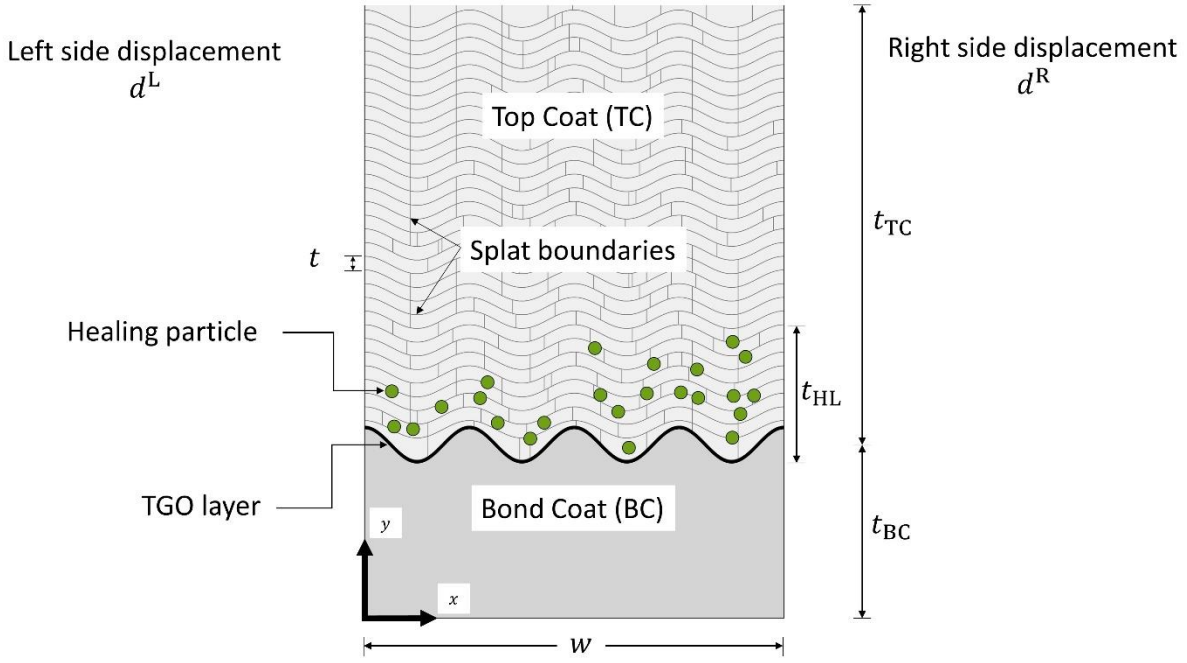

Figure 3.1: Unit cell for the self-healing TBC system

A MATLAB code has been utilized which takes the values of amplitude and wavelength of the TC/BC interface, number of lamellae and TBC dimensions as inputs in order to generate the TBC unit cell lattice [14,37]. Another MATLAB code has been developed which distributes the healing particles within the TBC domain by taking inputs such as the diameter, volume fraction of healing particles and the desired mean distance from the TC/BC interface. These two programs are used in conjunction in order to develop the TBC CAD file which is ready to be meshed. This CAD file consisting of the coordinates of TBC features is then uploaded to GMSH [88] which provides a convenient way of meshing the domain.

The region near the TC/BC interface encompassing the healing particles has been discretized with a fine mesh having a size of 1µm. This is because of the thermomechanical mismatch in properties near the TC/BC interface and the presence of healing particles which cause stress redistribution and eventually pave the way for initiation and propagation of cracks. On the other hand, in order to reduce the computational expense, the rest of the TBC domain has been discretized with a coarser mesh having a size of 2µm.

Subsequently, GMSH outputs a file which is then utilized as input by a MATLAB code that inserts cohesive elements throughout the mesh and assigns the loading and boundary conditions as well as the material properties to different element sets. Finally, the file generated by the MATLAB code is used as an input file in ABAQUS. Adding cohesive elements throughout the TBC domain ensures that the crack initiation and propagation is arbitrary and not dependent on the presence or absence of cohesive elements in specific regions of the TBC domain. A domain convergence analysis has been carried out for different values of TBC width w = 240µm, 360µm, 480µm, 600µm and 720µm. It has been observed that the change in the width normalized total crack size at failure is within 10% for w = 480µm, 600µm and 720µm. Hence the TBC width has been assigned the value w = 480µm for the rest of the analyses.

3.1.2 CRACK HEALING MECHANISM

In order to describe the system behaviour in response to cracking and subsequent healing, the cohesive zone based self-healing model developed by Ponnusami et al. [89] has been utilized. This model is based on a bilinear traction-separation law which takes as inputs the mode-I fracture energy and the normal fracture strength of the cohesive element material. The incorporation of self-healing and recovery of fracture properties is simulated with the help of a composite-based constitutive model in which the overall traction is described as a weighted sum of traction components of the original material and the healing material. An important advantage of the proposed model is the ability to simulate multiple and successive cracking and healing events. The model has been incorporated into the framework of the simulation in the form of an ABAQUS user-material subroutine.

3.1.3 SIMULATION OF TGO GROWTH

It is known that the exposure of TBCs to elevated temperature can lead to formation of thermally grown oxide (TGO) layer at the TC/BC interface due to high temperature diffusion of oxygen towards the metallic bond coat [14,74,90]. The TGO layer demonstrates higher stiffness and lower thermal expansion coefficient as compared with other TBC layers and thus can lead to thermomechanical mismatch stresses during thermal cycling.

In order to simulate the growth of the TGO layer and its effects as a function of number of thermal cycles, the above mentioned ABAQUS user-material subroutine utilizes a simplified TGO layer growth framework. Experimentally determined isothermal TGO growth curves depicting the thickness of the TGO as a function of number of thermal cycles [91,92] have been utilized and the data have been fitted with a logarithmic function which can be used in the subroutine in order to determine the TGO layer thickness as a function of number of thermal cycles.

It has been assumed that the TGO growth occurs during the dwell phase or in the course of exposure to elevated temperature. Additionally, an inward growth of the TGO has been proposed. This has been simulated by an incremental replacement of the BC material with TGO material. Therefore, the subroutine replaces the thermomechanical properties of the BC layer by those of the TGO material as a function of number of thermal cycles. This implies a presence of a mixture zone at the interface of the newly formed TGO layer and the existing BC layer. The properties of the elements within the mixture zone have been assigned with the help of a weighted average of the constitutive properties of the TGO and BC elements,

$$S = \omega S_{\mathrm{TGO}} + (1-\omega) S_{\mathrm{BC}} \tag{3.1}$$

Here, S represents the thermoelastic parameters whereas ω indicates the fraction of TGO material in the element belonging to the mixture zone. The utilized subroutine implements the incremental modification of properties by identifying the normal distance d_{c} of a BC element centroid from the sinusoidal TC/BC interface and then evaluates the constitutive properties based on the value of ω as follows,

$$\omega = \begin{cases} 0, & d_{\mathrm{c}} > t_{\mathrm{TGO}} + t_{\mathrm{mix}} \\ 1, & d_{\mathrm{c}} \leq t_{\mathrm{TGO}} \\ \dfrac{d_{\mathrm{c}} - t_{\mathrm{TGO}}}{t_{\mathrm{mix}}}, & t_{\mathrm{TGO}} < d_{\mathrm{c}} < t_{\mathrm{TGO}} + t_{\mathrm{mix}} \end{cases} \tag{3.2}$$

Here, t_{TGO} represents the current TGO layer thickness and t_{mix} indicates the thickness of the mixture zone which is equal to the size of an element at the interface between the TGO and BC layers.

3.1.4 MATERIAL PROPERTIES

The material properties assigned to different components of the TBC unit cell have been summarized in Table 3.1, and have been adopted from Krishnasamy et al. [17,18,19]. For the different TBC layers, a linear and isotropic thermoelastic response has been considered which can be represented using the parameters such as the Young's modulus E, thermal expansion coefficient α and the Poisson's ratio ν, whereas the fracture behaviour can be described with the help of the mode-I fracture energy G_{Ic} and the normal fracture strength σ_n. Additionally, the ratio between the mode-II and mode-I properties has been defined using the parameter γ. In order to demonstrate the lower fracture properties of the healed material as compared with the original undamaged material, the ratio of fracture properties of the healed material and those of the TC material has been set to 0.75.

Component	E (GPa)	ν	α (10^{-6} 1/°C)	σ_n (MPa)	G_{Ic} (N/mm)	γ
TC	80	0.15	12.5	150	0.006	4
BC	130	0.3	14.5	500	0.3	1
Healing particle	300	0.22	9.4	200	0.01	4
TGO	380	0.15	7	380	0.04	4
Substrate	200	0.28	16.5	-	-	-
Splat interface	-	-	-	50	0.001	4

Table 3.1: Summary of material properties [14]

3.1.5 MECHANISM OF HEALING ACTIVATION

In order to determine if the healing process has been activated due to a crack either reaching or originating from a healing particle, a Python based script has been utilized which consists of a crack tracking algorithm. This script is called at the end of every heating phase of a thermal cycle with the help of the subroutine URDFIL from ABAQUS, which can be utilized to access the results file at the end of an increment during an analysis [93]. Initially, the algorithm determines if any cohesive elements that are in contact with a healing particle have opened at the end of the heating phase. A cohesive element is considered as opened if it dissipates at least 10% of its fracture energy.

This criterion has been chosen based on simulations which were compared with experimental solutions in order to calibrate material properties and simulation parameters [14]. After the initial step, the algorithm identifies the failed cohesive elements that are in contact with the previously identified cracked elements in order to determine the crack path as well as the total cracked area. The value for the total cracked area is compared with the available healing volume in the healing particle in order to update the available healing volume for the subsequent steps.

3.1.6 ARTIFICIALLY ACCELERATED THERMAL CYCLING

Most of the applications of TBCs involve a typical thermal loading cycle consisting of three distinct phases: heating, dwell and cooling. To this end, the simulation framework considers a heating phase in which the temperature is increased from 30°C (nominal ambient temperature) to 1100°C (test temperature). This is followed by the dwell phase in which the TBC is exposed to constant elevated temperature of 1100°C. Finally, the cooling process involves reduction of temperature from 1100°C to 30°C. It has been assumed that during the dwell phase, the TBC system does not experience any thermomechanical stresses since the elevated temperature is considered to be the coating deposition temperature. Consequently, the cooling phase is responsible for the generation of thermomechanical stresses due to the mismatch in thermal expansion coefficients between different components of the TBC system.

Experimental results for determination of TBC lifetime indicate that in general the lifetime is of the order of several hundred thermal cycles. However, since it is computationally expensive to simulate the crack initiation and growth to failure considering the modelling parameters, the self-healing TBC model considers an accelerated thermal loading state. In order to alleviate the computational cost while capturing the cyclic damage and healing, an artificially accelerated TGO growth has been considered where one simulated cycle represents the TGO growth of 25 actual cycles. The logarithmic curve used to fit the experimentally obtained TGO growth results as a function of actual and accelerated thermal cycles can be observed in Figure 3.2. In this way, the considered self-healing TBC model explicitly models the thermal cycles by considering uniform temperature distribution. The effects of the rates of heating and cooling are not considered as the micromechanical model used is essentially a static model. Also, the material properties are taken to be temperature and time-independent.

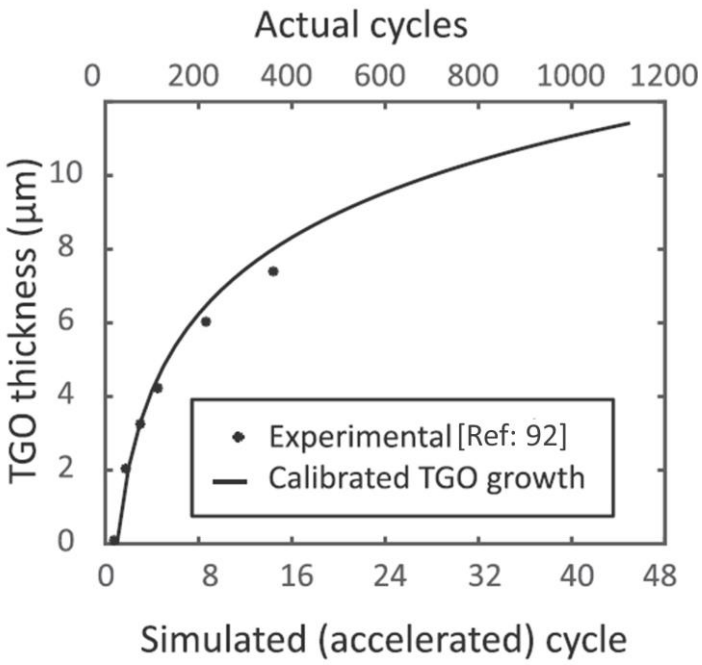

Figure 3.2: Calibrated TGO growth as a function of number of thermal cycles [14,92]

Complete failure of the TBC system is considered to have taken place when 90% of the TC layer has separated from the TC/BC interface or the TGO layer. For the purpose of post-processing, a Python script has been utilized which accesses the output database that is generated during the simulation. This script identifies the coordinates of the cracked and healed elements for each step of the thermal cyclic loading. A MATLAB code has been developed which reads the data consisting of the coordinates and provides the total crack length, length of the largest continuous crack and number of cracks as a function of number of computational thermal cycles as well as the TBC crack patterns at failure. An example of an output for the same can be observed in Figure 3.3. In Figure 3.3(b), the healed cracks are plotted in blue whereas the red colour indicates the active cracks.

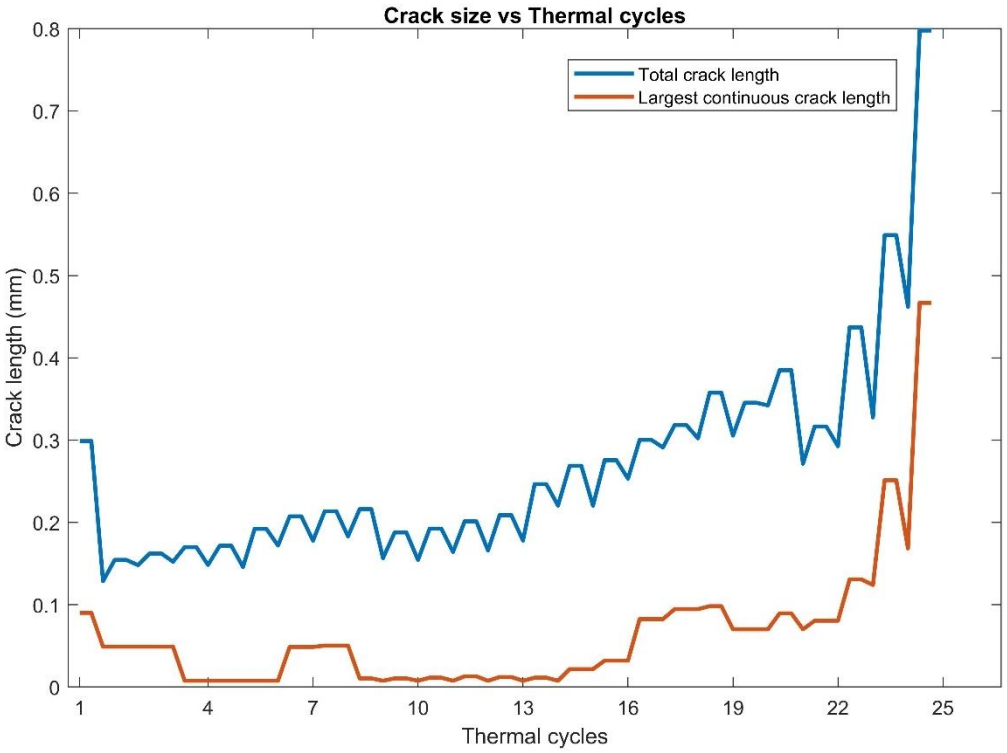

Figure 3.3(a): Crack growth as a function of number of thermal cycles

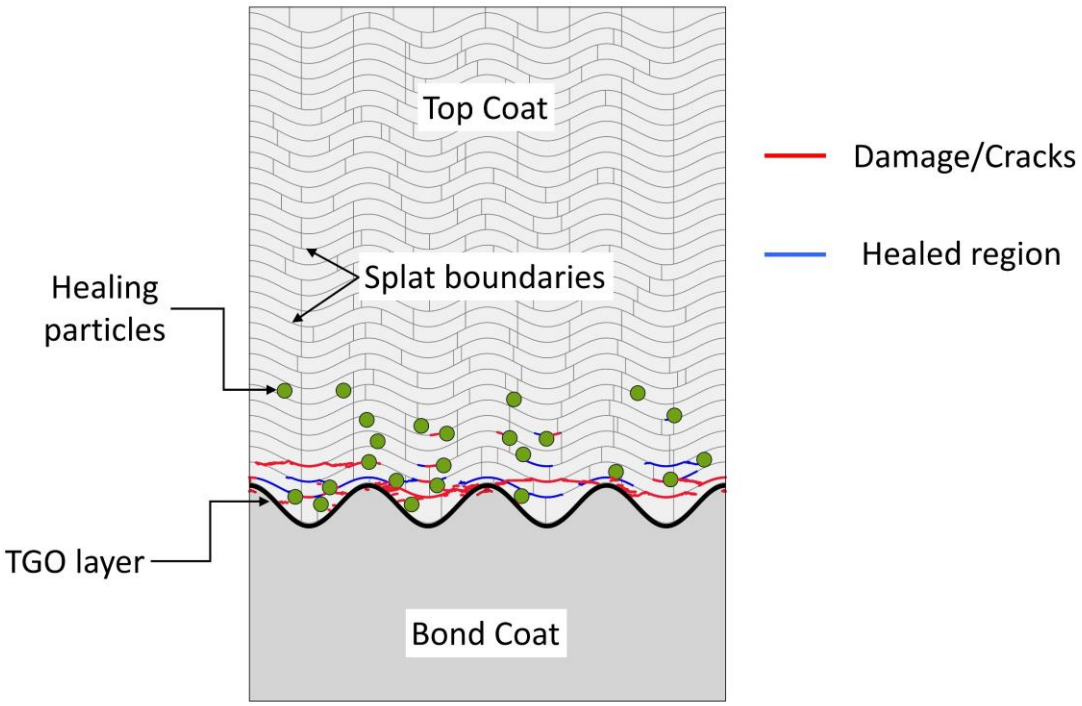

Figure 3.3(b): Crack pattern at TBC failure

3.2. TRAINING THE SURROGATE MODEL

3.2.1 INPUT VARIABLE DISTRIBUTIONS

In order to develop a surrogate model for the computationally expensive numerical simulations, the number of computational thermal cycles to failure is considered to be the quantity of interest. As identified in Section 2.4, the input parameters for the polynomial chaos expansion (PCE) are the TC/BC interface amplitude, the TGO growth rate, mean distance of healing particles from the TC/BC interface and the volume fraction and diameter of healing particles. For the purpose of developing the PCE based surrogate model, the first step is to obtain the orthogonal polynomials with the help of the joint probability distribution of the input parameters. The joint probability distribution can be derived by defining the individual input variable distributions, which in turn can be decided based on experimental observations, existing information and expert understanding [69]. The growth rate of TGO thickness as a function of number of thermal cycles has been quantified with the help of a multiplying coefficient in the logarithmic function used to fit the experimentally obtained results. Figure 3.4 gives an example of how varying the multiplying coefficient helps to modify TGO growth rate.

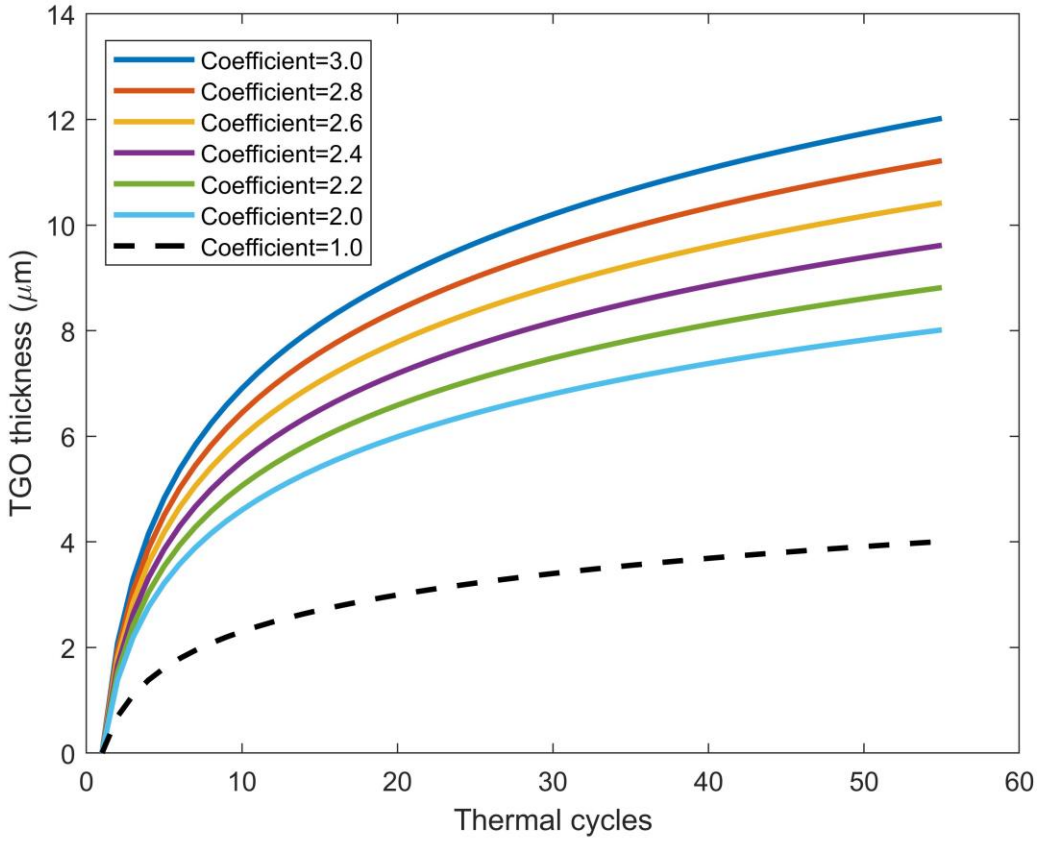

Figure 3.4: Variation of TGO growth rate

In order to observe the impact of the variation of the interface amplitude, a uniform distribution of values with bounds [15,25] µm is considered based on finite element simulations [71-73] and the design rules as developed in the SAMBA project [109]. The multiplying coefficient of TGO growth rate has been assumed to vary uniformly between [2.5,3]. This distribution has been decided with the help of prior simulations which were carried out for a range of TGO growth rate coefficient values in order to determine the viability of duration of simulations for the available computational resources. A normal distribution is proposed for the volume fraction of healing particles with a mean value and standard deviation of 7.5% and 1% respectively. For the purpose of determining the sensitivity of TBC lifetime to diameter of healing particles, the diameter value is varied uniformly between the bounds [10,20] µm. The value for the mean distance of healing particles from the TC/BC interface has been distributed uniformly between [45,80] µm such that the healing particles encompass the entire healing layer thickness for the considered range of volume fraction and diameter of healing particles. The input variable distributions considered in the project have been summarized in Table 3.2.

Input variable	**Unit**	**Distribution**
Interface amplitude	µm	Uniform ~ $[15, 25]$
TGO growth coefficient	-	Uniform ~ $[2.5, 3.0]$
Volume fraction of healing particles	%	Normal ~ $(7.5, 1)$
Diameter of healing particles	µm	Uniform ~ $[10, 20]$
Mean particle distance	µm	Uniform ~ $[45, 80]$

Table 3.2: Statistical characteristics of uncertain input parameters

3.2.2 SELECTING THE ORDER OF POLYNOMIAL CHAOS EXPANSION

In order to develop and train the surrogate model, *Chaospy* has been utilized, which is a Python-based toolbox used for uncertainty quantification using polynomial chaos expansion [94]. It can be used to generate random input variable distributions, obtain orthogonal polynomials, derive samples from the defined distributions as well as generate useful statistical metrics. Chaospy has been employed to obtain the joint probability distribution function by defining the input variable distributions as described in Table 3.2. Obtaining the orthogonal polynomial basis from the joint probability distribution function requires the prior definition of the PCE order. It has been observed that there are no specific guidelines to set a particular order since the optimum order may vary in different underlying models [45]. For a specific number of input variables and an oversampling ratio, the chosen PCE order also affects the number of samples to be generated for training the surrogate model as indicated by Equation (2.6). Table 3.3 employs this equation and gives an idea about the number of samples required for a PCE order n and number of input variables k for an oversampling ratio of 2.

n \ k	1	2	3	4	5	6
1	4	6	8	10	12	14
2	6	12	20	30	42	56
3	8	20	40	70	112	168

Table 3.3: Variation of number of sampling points with PCE order (n) and number of input variables (k)

Since each sampling point corresponds to a computationally expensive simulation, a trade-off between available computational resources and the accuracy of surrogate model is required in order to decide the PCE order. For the present work, a PCE order n=2 has been chosen such that it satisfies the computational constraints and is also able to capture the possible non-linearities in the response of the underlying model as well as the interactions between the input variables. It has also been observed in literature that a second-order PCE is able to demonstrate sufficient accuracy in determining the mean and standard deviation of the response whereas a higher order might be required in order to accurately determine higher order statistical moments such as skewness and kurtosis [95].

3.2.3 GENERATION OF SAMPLING POINTS

Once the input variable distributions and the PCE order have been defined, Chaospy can be utilized to obtain the joint probability distribution of the variables, which consequently serves two purposes. Firstly, it can be used to obtain the orthogonal polynomial basis. Secondly, it can be used to sample points from the input variable distribution space which will be utilized by the finite element model in order to provide the TBC lifetimes. Hence, for a PCE of order $n = 2$ and number of input variables $k = 5$, it can be observed from Table 3.3 that a total of 42 samples are required. These samples can be generated from the joint distribution of input variables with the help of Latin hypercube sampling (LHS). This is a sampling approach which is able to encompass the input design space and hence it provides representative samples from the entire stratification of variables.

Each sample point corresponds to a particular value of the TC/BC interface amplitude, TGO growth rate coefficient, volume fraction and diameter of healing particles as well as the mean distance of healing particles from the TC/BC interface. The value of the interface amplitude can be varied within the MATLAB code which is used for geometry generation whereas the TGO growth rate coefficient can be modified within the user subroutine before submitting the job for finite element simulation. Additionally, a MATLAB code has also been developed which provides the distribution of healing particles for a desired value of mean distance from the TC/BC interface by taking the volume fraction and diameter of healing particles as inputs.

3.2.4 POST-PROCESSING OF THE SURROGATE MODEL

Once the quantity of interest, being the TBC lifetime, has been obtained for each of the samples, the vector of TBC lifetimes can be used to train the surrogate model and obtain the PCE coefficients. The surrogate model can then be utilized in conjunction with Monte Carlo simulation in order to obtain the probability density function as well as statistical characteristics such as the expected value and standard deviation of the TBC lifetime. A Python script has been developed which provides the above-mentioned statistical outputs. The trained model can also be used to obtain the sensitivity indices which indicate the contribution of individual input variables to the variance in TBC lifetime. The prediction accuracy of the surrogate model can be determined with the help of techniques such as leave-one-out cross validation [96] or k-fold cross validation for which scripts have been developed which utilize the *scikit-learn* package in Python [97]. Figure 3.5 provides the workflow of the overall computational procedure implemented in the project.

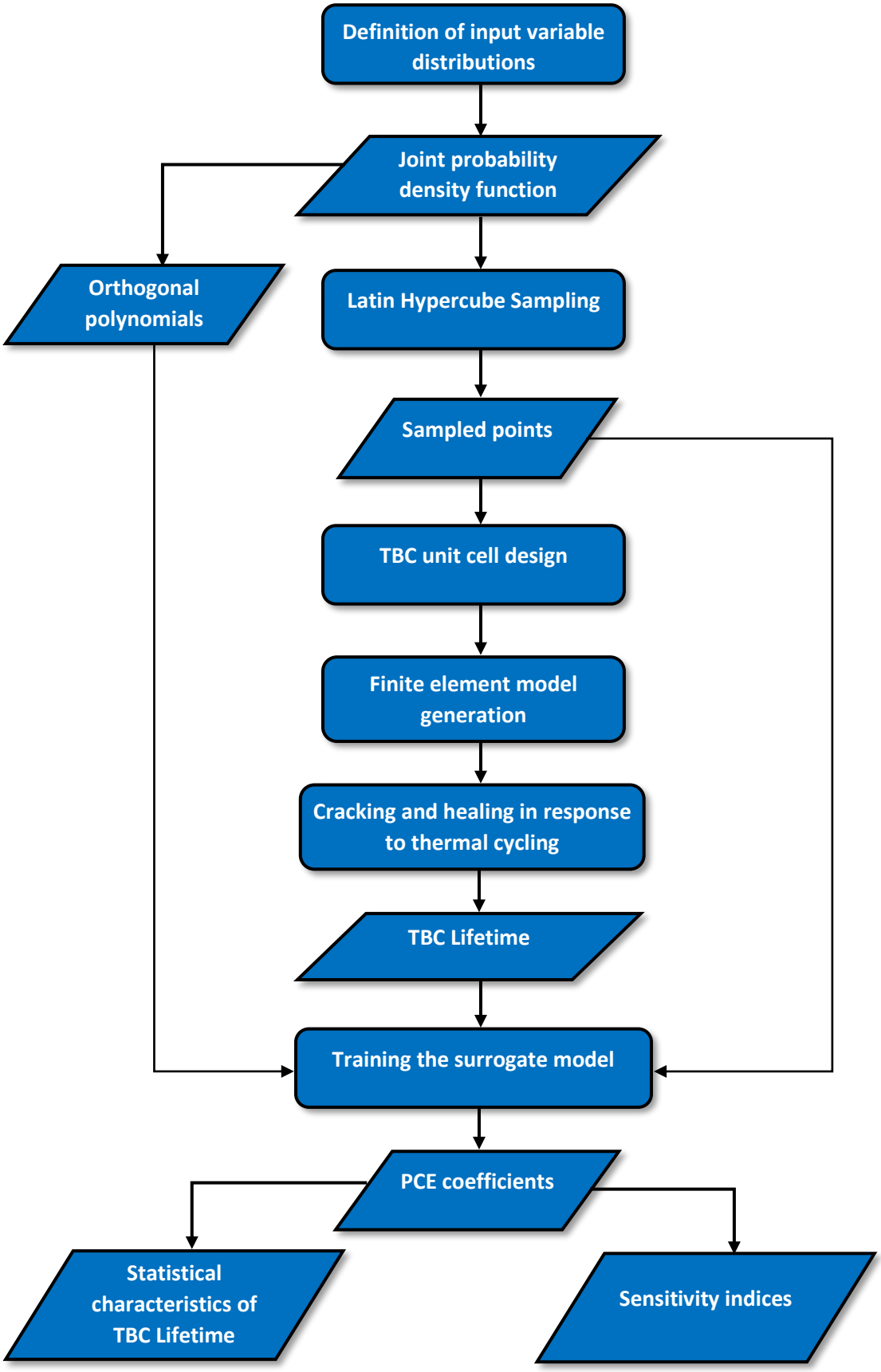

Figure 3.5: Overall computational workflow

4

RESULTS AND DISCUSSION

This chapter provides the characteristics of the trained PCE-based surrogate model. Initially, the ability of the model to fit the actual data has been described with the help of a residual plot. This is followed by a validation of the predictive performance of the model. The trained model has also been compared with another PCE model having order = 1 in order to demonstrate the relative prediction capabilities. A sensitivity plot has been provided which compares the impact of each of the considered input variables on the variation in TBC lifetime. An additional surrogate model is developed for the case of the benchmark TBC without healing particles in order to make a comparison with the surrogate model developed for TBC with healing particles and determine the effect of use of self-healing particles on the expected value of TBC lifetime and the underlying scatter in thermal fatigue life.

4.1. RESIDUAL PLOT

TBC lifetime results are obtained by carrying out finite element simulations at the sampled points. These data points are utilized to train the surrogate model as a consequence of which the PCE coefficients are derived. In order to determine how well the trained model fits the actual data points and to have an indication regarding the quality of fit, a residual plot is presented in Figure 4.1. In this plot, the X-axis consists of the actual data points whereas the corresponding Y-coordinates indicate the residual or the error between the actual values and those produced by the surrogate model. The residual plot can be utilized for two purposes. Firstly, it indicates the goodness of fit that can be achieved with the trained model. Secondly, it describes whether the variation in the output can be explained by the input variables. For instance, if there exists an observable trend or non-randomness in the residuals then this implies that the input variables are not sufficient to describe the variation in the output. As a result, this calls for improvement in the model. However, the obtained plot indicates that the residual data points are scattered randomly around the zero line which supports the validity of the trained model [98, 99].

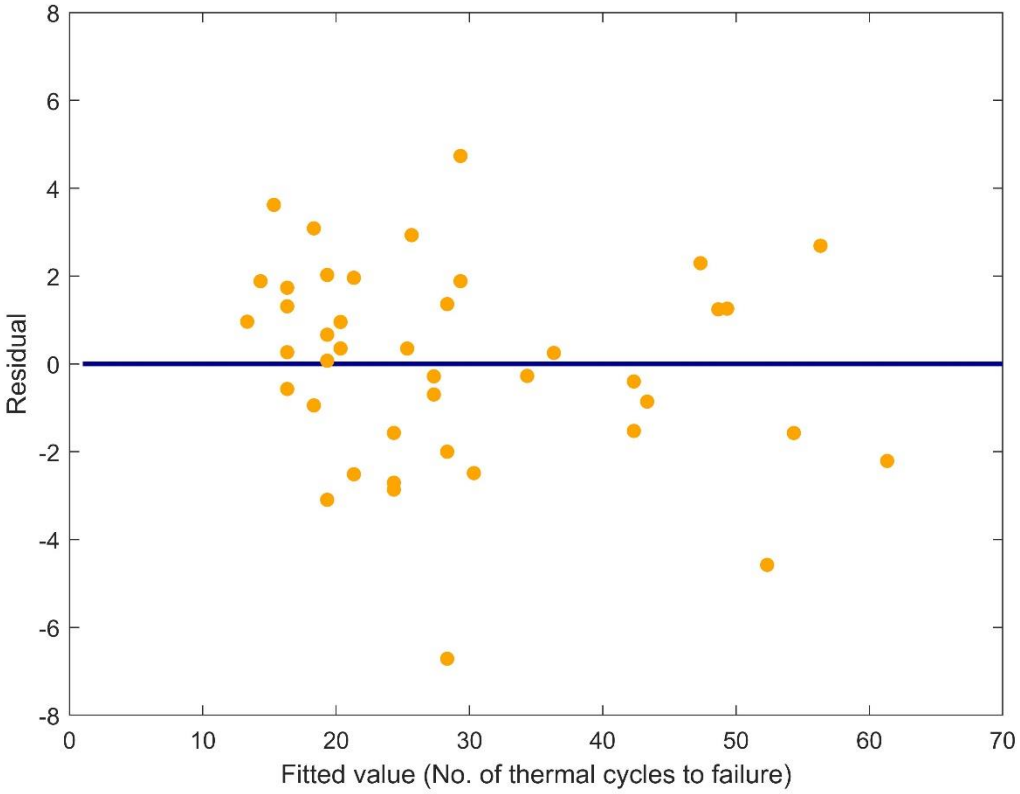

Figure 4.1: Residual plot for the surrogate model

Additionally, the quality of fit can also be assessed with the help of the coefficient of determination R^2. Consider a model Y whose limited number of runs on the sampled points $S = (s^{(1)}, s^{(2)}, s^{(3)}, \dots s^{(N)})$ can be used to train the surrogate model $\check{Y}$. Here, $s^{(i)}$ represents a particular value for each of the considered input variables. The training error can be defined in the following manner [100]:

$$Err_{train} = \frac{1}{N}\sum_{i=1}^{N}\left(Y(s^{(i)}) - \check{Y}(s^{(i)})\right)^2 \tag{4.1}$$

The coefficient of determination can be defined as follows:

$$R^2 = 1 - \frac{Err_{train}}{\check{V}} \tag{4.2}$$

Here, $\check{V}$ represents the variance observed in the responses of the trained surrogate model. However, as the cardinality or the number of terms in the PCE (Q) increases, the number of sampled points (N) also increases which can lead to overfitting of the model to the actual data points.

This phenomenon can lead to increased prediction errors while using the surrogate model on new data. In order to take this into account, the coefficient of determination can be modified and adjusted to the number of PCE coefficients (Q) as follows [45]:

$$R^2_{adjusted} = 1 - \left(\frac{N-1}{N-Q-1}\right)(1-R^2) \tag{4.3}$$

The following results have been obtained for the trained surrogate model:

$$R^2 = 0.97$$

$$R^2_{adjusted} = 0.94$$

From the obtained value of the adjusted coefficient of determination, it can be observed that despite the underlying complexities and non-linearities in the self-healing TBC model, the surrogate model is able to fit well to the actual data points. However, it has been observed that the adjusted coefficient of determination overpredicts the accuracy of approximation [101]. Also, evaluation of residuals and the quality of fit does not indicate how well the trained model will perform on new data or unseen sample points.

4.2. LEAVE-ONE-OUT CROSS VALIDATION

In order to determine the predictive performance of the surrogate model, Leave-one-out (LOO) cross validation technique has been implemented. According to this method, initially a surrogate model $\check{Y}^{(\sim i)}$ is built by training it on all but the i^{th} sample point. This metamodel is then used to predict the value of the original model Y at the i^{th} observation and the prediction error is evaluated:

$$\Delta^{(i)} = Y\left(s^{(i)}\right) - \check{Y}^{(\sim i)}\left(s^{(i)}\right) \tag{4.4}$$

This process is repeated for all the sample points and the predicted residual sum of squares [100] or the leave-one-out cross validation error is calculated as follows:

$$Err_{LOO} = \frac{1}{N}\sum_{i=1}^{N} {\Delta^{(i)}}^2 \tag{4.5}$$

The LOOCV algorithm has been represented in Figure 4.2.

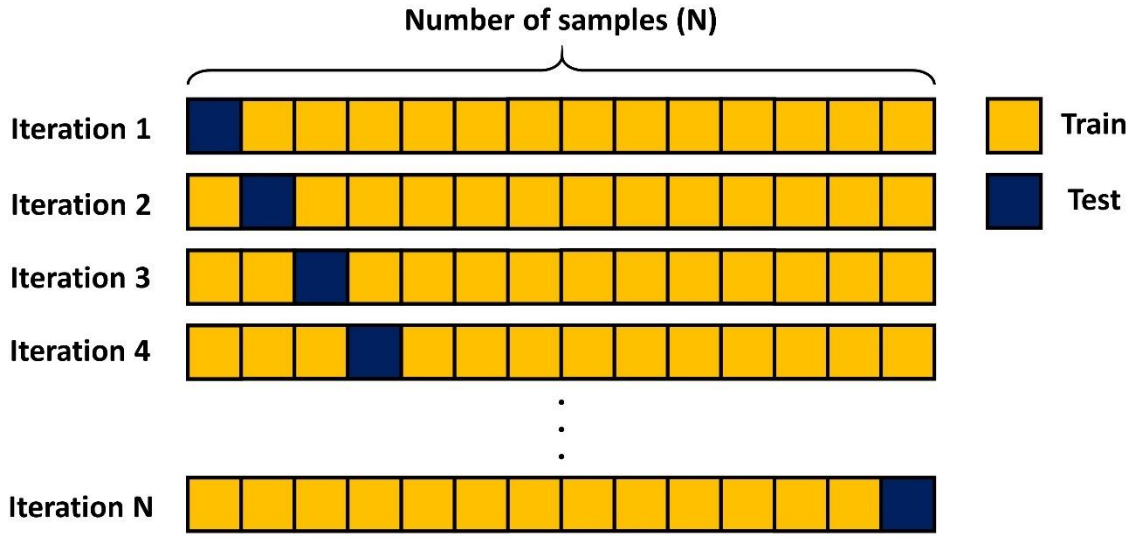

Figure 4.2: Leave-one-out cross validation process

In order to visualize the advantages of developing a surrogate model with a PCE order = 2, the current model ($\check{Y}$) has been compared with a model developed using a PCE order = 1 ($\check{Y}_1$). Initially, LOOCV error has been evaluated for the model $\check{Y}_1$ considering the same sample points that were utilized for training the model $\check{Y}$. The following results have been obtained:

$$Err_{LOO}(\check{Y}) = 28.9$$

$$Err_{LOO}(\check{Y}_1) = 41.2$$

However, it can be observed from Table 3.3 that for an oversampling ratio = 2, the number of sample points required for a PCE order = 1 and number of input variables = 5 is 12. Hence, as an additional verification step, 12 samples have been chosen at random from the initial sample space and LOOCV has been performed for those 12 samples. This process is repeated until the entire initial sample space has been represented for the case of PCE order = 1. Finally, the mean LOOCV error has been evaluated.

$$Mean\ Err_{LOO}(\check{Y}_1) = 62.3$$

From the above results, it can be observed that a surrogate model developed with a PCE order = 2 demonstrates a better predictive performance than the one developed with a PCE order = 1.

4.3. TRAINED SURROGATE MODEL

Equation 4.6 states the final polynomial function derived capturing the direct and coupled dependencies of the lifetime on model parameters.

$$\begin{aligned}\check{Y} \quad = \quad & 470.53 + 13.73x_5 - 1.56{x_5}^2 - 1.19x_4 + 0.01x_4x_5 + 0.01{x_4}^2 - 8.02x_3 \\ & -3.75x_3x_5 + 0.05x_3x_4 + 0.27{x_3}^2 + 23.44x_2 - 9.63x_2x_5 - 0.01x_2x_4 + 0.12x_2x_3 \\ & +0.79{x_2}^2 - 38.14x_1 + 4.78x_1x_5 - 0.01x_1x_4 + 0.27x_1x_3 - 0.46x_1x_2 + 0.53{x_1}^2\end{aligned} \quad \ldots (4.6)$$

In the above equation, $\check{Y}$ represents the TBC lifetime in number of computational thermal cycles. The input terms are summarized along with their respective considered distributions as follows:

x_1	=	TC/BC interface amplitude	Uniform ~ [15,25] µm
x_2	=	Healing particle volume fraction	Normal ~ (7.5,1) %
x_3	=	Healing particle diameter	Uniform ~ [10,20] µm
x_4	=	Mean distance of healing particles from TC/BC interface	Uniform ~ [45,80] µm
x_5	=	TGO growth coefficient	Uniform ~ [2.5,3]

This equation represents the surrogate model generated using the orthogonal polynomials derived from the Askey scheme of polynomials [57, 58]. The coefficients in the model have been obtained with the help of the method of least squares. This method utilizes the finite element model responses at the sampling points obtained using Latin hypercube sampling. This trained model can be used in conjunction with Monte Carlo sampling in order to derive the probability density function of the self-healing TBC lifetime. It can also be used to observe the relative impact of each of the input variables on the variation in the output or the sensitivity indices. Additionally, after determination of the most sensitive input variables, the surrogate model can be helpful to obtain the statistical characteristics of the variation of TBC lifetime as a function of the sensitive variable while the uncertainties in the remaining variables are propagated through the surrogate model. This implies that controlling the value of the sensitive variables while designing the self-healing TBCs will help in the determination of the reliability of the surrogate model output in the form of standard deviations.

4.4. SENSITIVITY ANALYSIS

In order to obtain the relative contribution of each input variable to the output variance, a sensitivity analysis can be carried out using the trained surrogate model. A commonly utilized approach to evaluate sensitivity indices is Sobol's method. Using this method, the output variance is decomposed into contributions associated with each of the input variables. Suppose the output Y is a function of input variables $(X_1, X_2, X_3 \dots X_N)$. To calculate the sensitivity index of X_i, the method proposes initially fixing the variable at a particular value $(X_i = c_i)$ and then calculating the change in output variance or the conditional variance:

$$\mathrm{V}_{X\sim i}(Y|X_i = c_i)$$

Here, the output variance $\mathrm{V}_{X\sim i}$ is calculated by considering the uncertainties in all but the i^{th} input variable. Since X_i also depicts uncertainty in terms of a distribution of values, a mean of the above-mentioned conditional variance is evaluated over the distribution of X_i in order to obtain the expected value:

$$\mathrm{E}[\mathrm{V}_{X\sim i}(Y|X_i)]$$

Since the conditional variance is calculated over all the input variables other than X_i, it can be understood that smaller the expected value of the conditional variance, more sensitive is the output response to changes in X_i. Also, according to the law of total variance [102],

$$\mathrm{V}(Y) = \mathrm{E}[\mathrm{V}(Y|X)] + \mathrm{V}(\mathrm{E}[Y|X])$$

Therefore,

$$\mathrm{V}(Y) = \mathrm{E}[\mathrm{V}_{X\sim i}(Y|X_i)] + \mathrm{V}(\mathrm{E}_{X\sim i}[Y|X_i]) \tag{4.7}$$

Dividing both sides of the equation by $\mathrm{V}(Y)$,

$$1 = \frac{\mathrm{E}[\mathrm{V}_{X\sim i}(Y|X_i)]}{\mathrm{V}(Y)} + \frac{\mathrm{V}(\mathrm{E}_{X\sim i}[Y|X_i])}{\mathrm{V}(Y)} \tag{4.8}$$

The second term on the RHS of Equation (4.8) is defined as the first order sensitivity index which is representative of the influence on the output variance of each input variable taken alone [95]. The Chaospy module in Python also provides the total sensitivity indices which include the possible interactions of input variables and hence their joint effect towards the output variance. Figure 4.3 provides a summary of the obtained sensitivity indices.

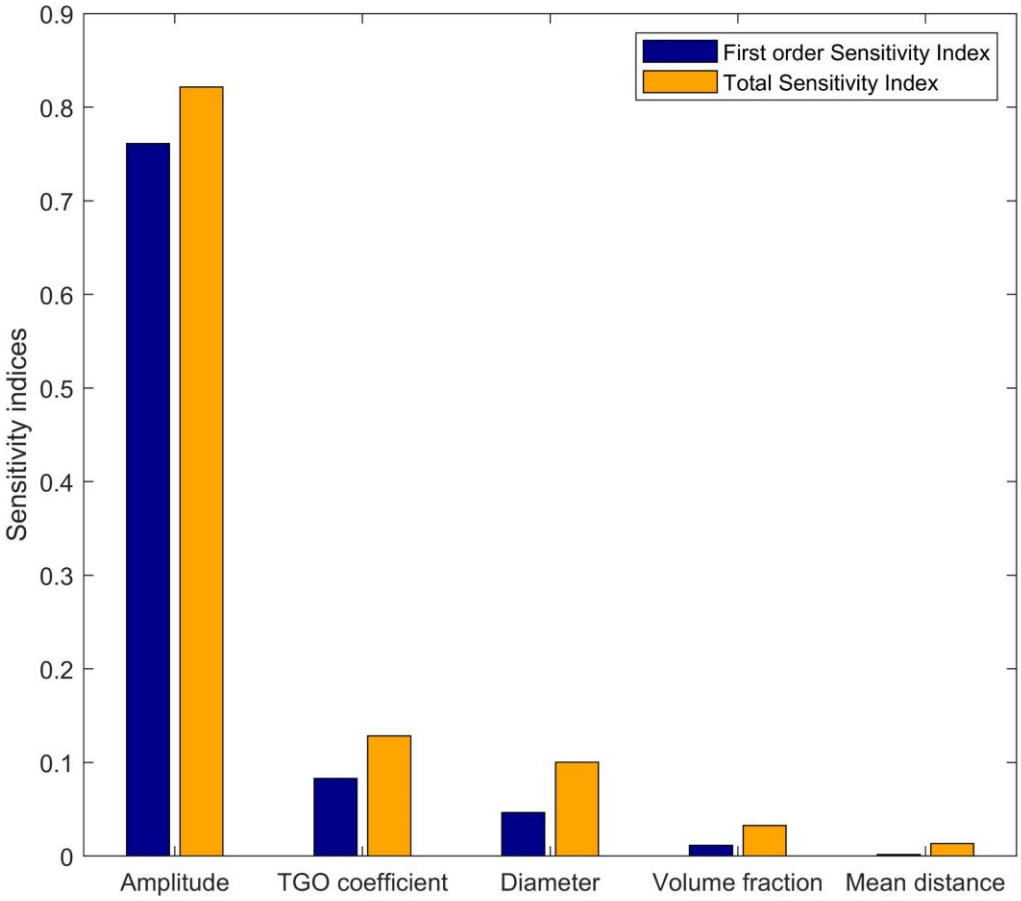

Figure 4.3: Sensitivity indices

It can be observed that the TC/BC interface amplitude is the main contributor towards the variance in TBC lifetime. This implies that relatively small changes in the value of the amplitude will result in a high change in the TBC lifetime. In order to observe how the output variance depends on the input variable sensitivity, Figure 4.4 provides the probability density functions developed using the TBC lifetime responses from the surrogate model. Two scenarios have been compared. The first one considers the uncertainties in all the input variables and hence provides a general response PDF. In the second case, the input variable having the highest sensitivity index or the interface amplitude has been fixed at its mean value while the uncertainties in the rest of input variables have been taken into account.

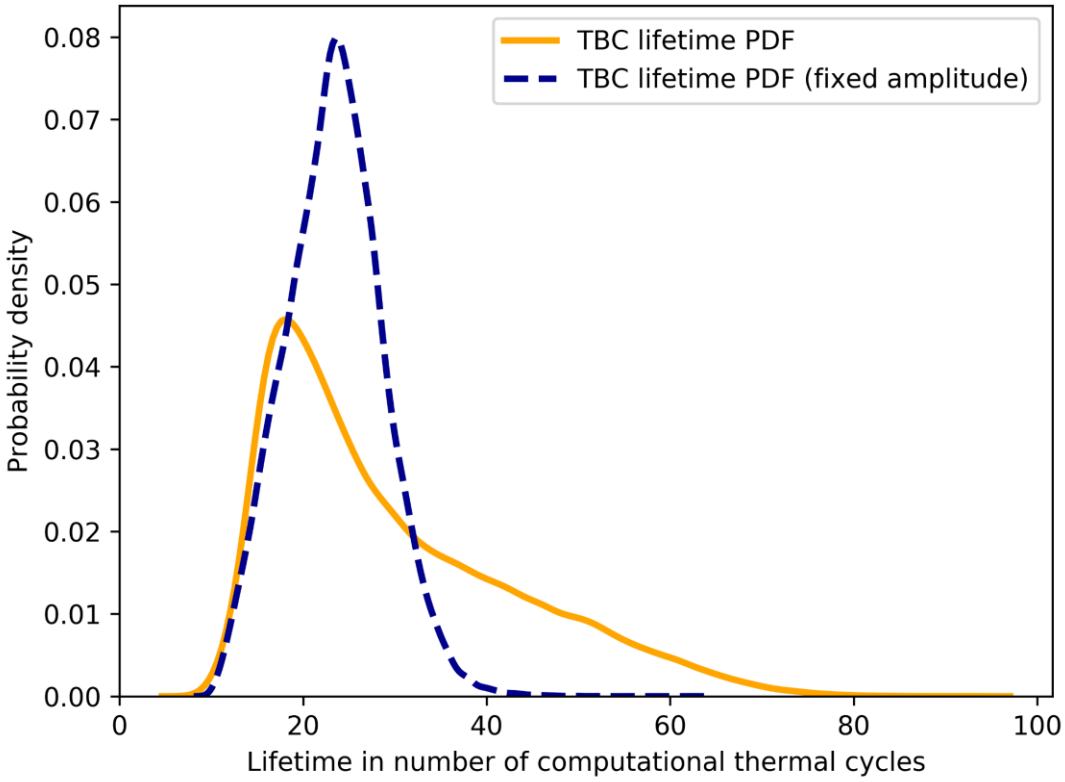

Figure 4.4: Influence of fixing the input variable with the highest sensitivity index

In order to compare the degree of variance in the two scenarios, the coefficient of variation (COV) [45] has been calculated for both cases. COV is also known as the relative standard deviation which is defined as the ratio of the standard deviation to the mean value. COV for the first case has been found out to be 45% whereas the second case describes a COV of 22%. Since the interface amplitude value is the most significant contributor to the output variance, fixing its value reduces the dispersion in the TBC lifetime response. This implies that incorporating focussed attempts to control the interface amplitude value will help to increase the reliability of TBC lifetime results.

4.5. UNCERTAINTY PROPAGATION PLOTS

In order to visualize how the output changes while a particular input variable is controlled, the variation in TBC lifetime is plotted in Figure 4.5 as a function of each variable X_i while the uncertainties in the remaining input variables $X_{\sim i}$ have been propagated through the surrogate model.

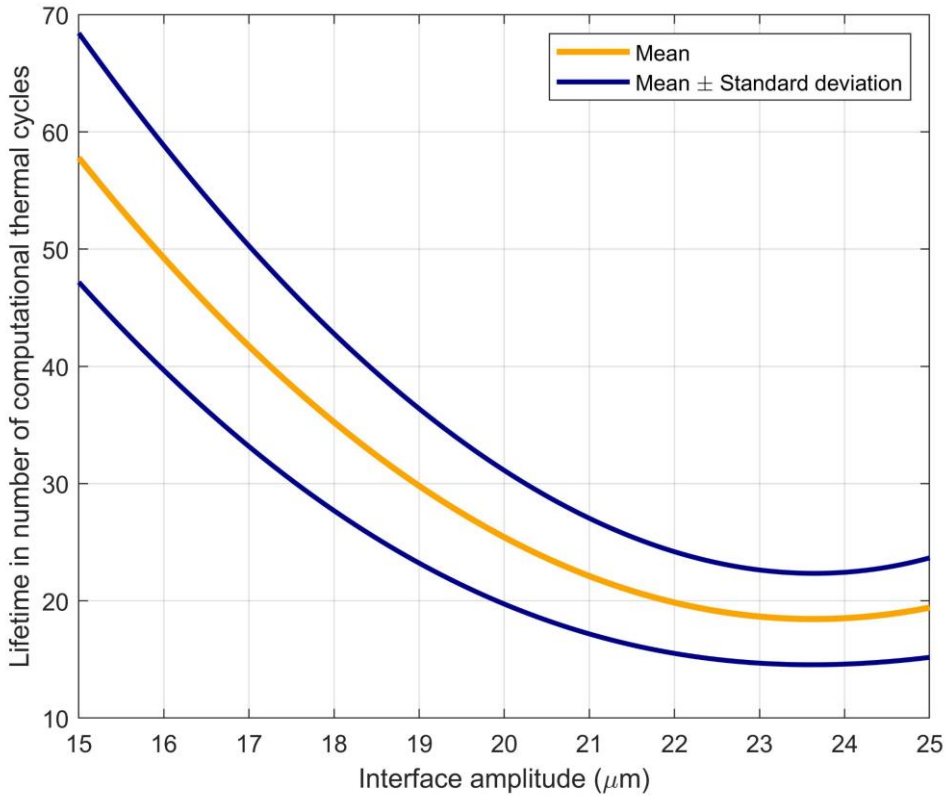

Figure 4.5(a): TBC lifetime vs Interface amplitude

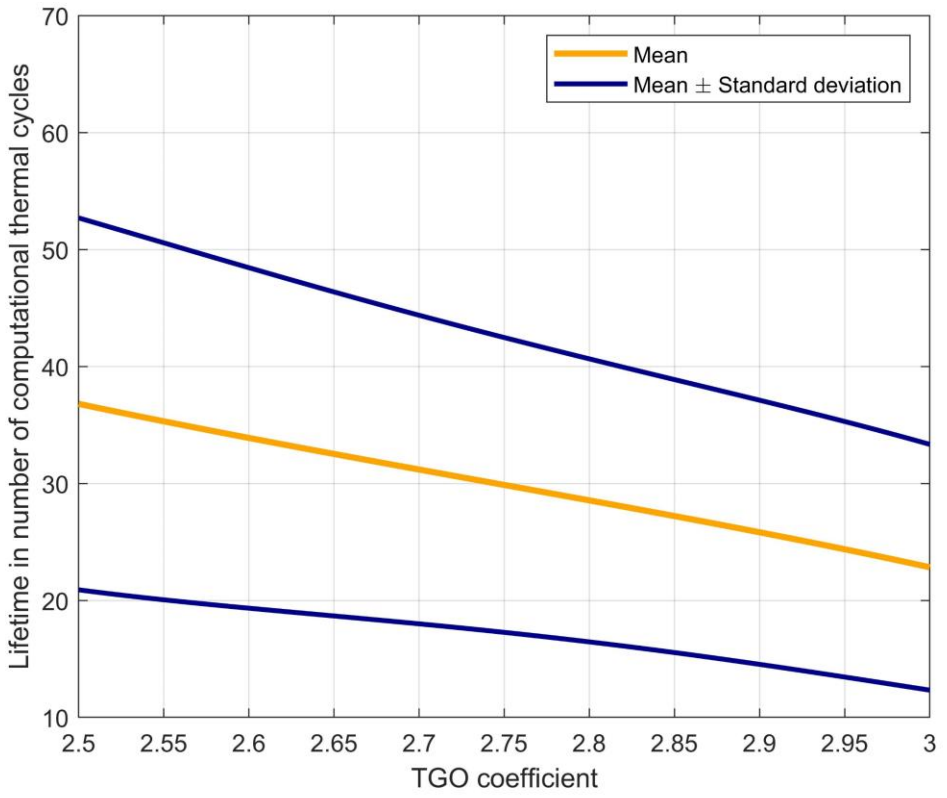

Figure 4.5(b): TBC lifetime vs TGO coefficient

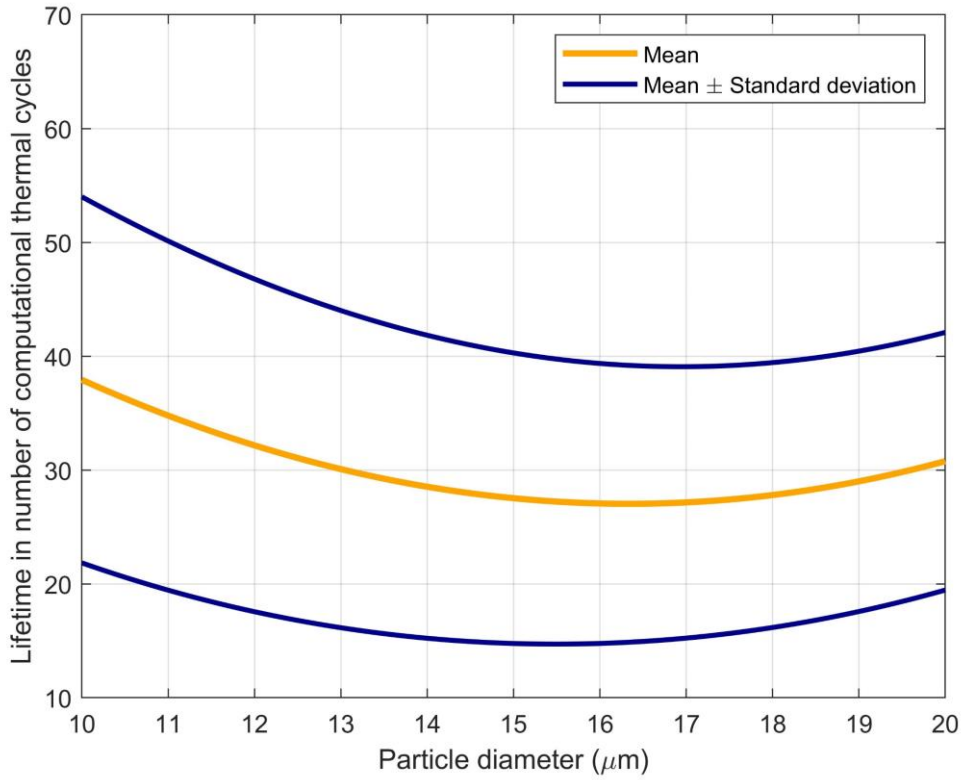

Figure 4.5(c): TBC lifetime vs Particle diameter

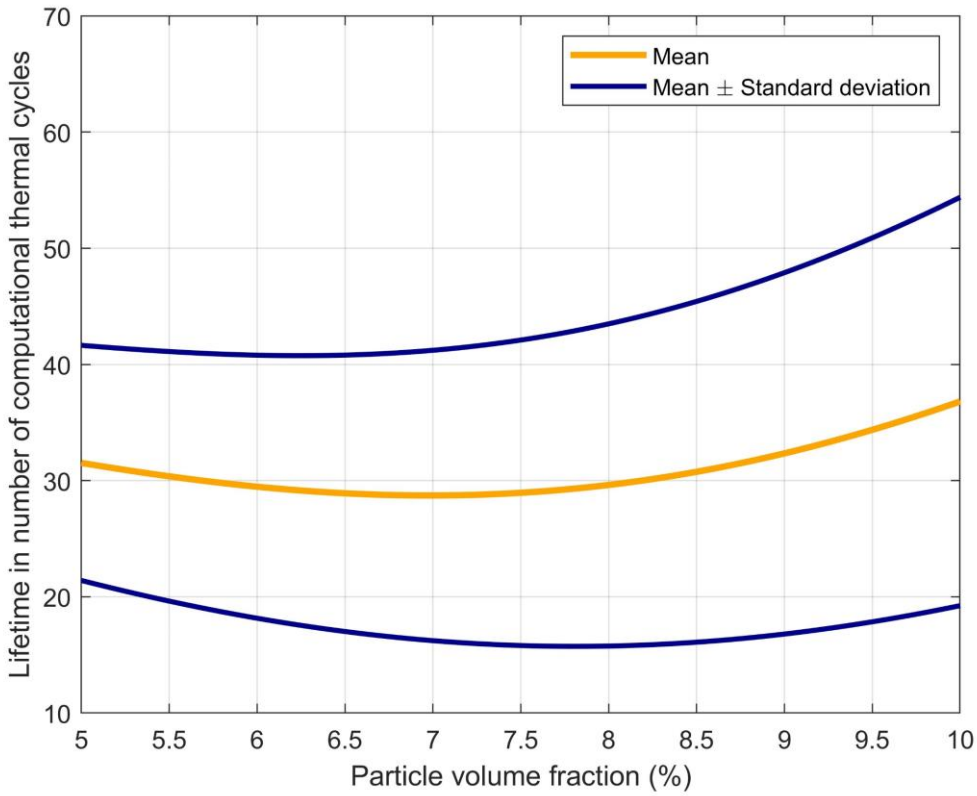

Figure 4.5(d): TBC lifetime vs Particle volume fraction

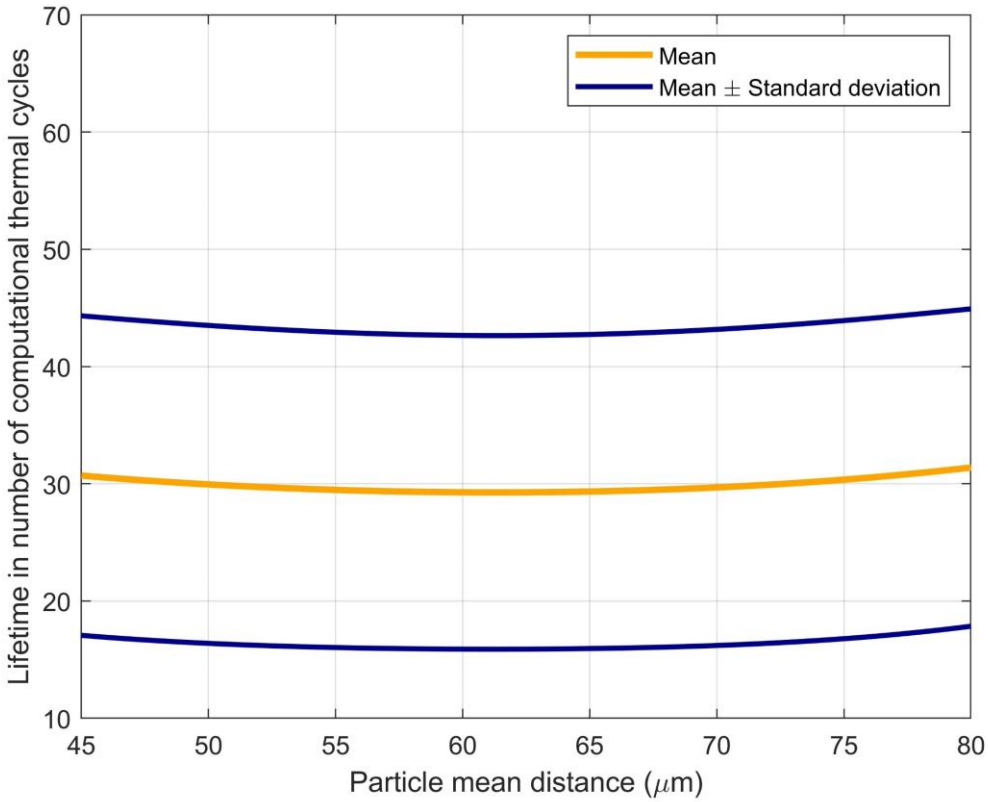

Figure 4.5(e): TBC lifetime vs Particle mean distance from TC/BC interface

The above of set of figures represents the trend of the response surface generated using the Askey scheme of polynomials as mentioned in Table 2.1 with respect to each of the input variables. Figure 4.5(a) confirms the result from Figure 4.3 that the TBC lifetime varies the most with changes in the interface amplitude value. It also indicates that a decrease in interface amplitude value will lead to a gain in TBC lifetime. This observation has also been made by several researchers who have carried out two-dimensional as well as three-dimensional finite element studies to understand the impact of roughness or the TC/BC interface topography on damage growth and lifetime of TBCs. Studies have indicated that an increase in the value of interfacial waviness or roughness leads to increased magnitude of stresses at the TC/TGO and TGO/BC interfaces as well as the TC layer, thus affecting the fatigue life of TBCs [104, 105]. It has also been observed that the development of damage as a result of thermal cycling is directly proportional to the interface roughness values [87]. This implies that in order to predict the TBC lifetime, special efforts need to be taken while measuring the value of interface amplitude. Additionally, focus should be given upon controlling the feedstock powder size during manufacturing of TBCs to obtain a desirable value of interface amplitude.

Figure 4.5(b) describes the variation of TBC lifetime as a function of the TGO growth coefficient. It can be observed that the expected value of TBC lifetime reduces with an increase in the TGO growth coefficient value. Experimental studies have indicated that the fracture toughness of the TGO reduces with progression of thermal cycles which paves the way for easier crack growth and coalescence [106]. As this reduction in fracture toughness will occur at a higher rate for a higher rate of TGO growth, the number of cycles required for delamination will reduce, consequently reducing the TBC lifetime. Investigations have also indicated the effects of TGO thickness values on stress redistribution and damage growth in TBCs [74-77]. Thus, efforts can be implemented in order to reduce the TGO growth rate. It has been observed that the TGO growth rate can be controlled by modifying the BC manufacturing process [79] or by carrying out a pretreatment of the BC which constrains the initiation and growth of cracks between the TC and TGO layers [107].

Figures 4.5(c), (d) and (e) also agree with the obtained sensitivity indices in such a way that there exists less variation in TBC lifetime across the considered ranges of healing particle diameter, particle volume fraction and the particle mean distance from TC/BC interface respectively. This indicates that for the considered ranges of the values of variables associated with healing particles, controlling the manufacturing process may not yield tangible benefits in prediction of TBC lifetime. Instead, the number of available healing sites, which is derived from the combination of the three above-mentioned variables, determines whether a growing crack will be arrested and healed, thus resulting in a subsequent extension of TBC lifetime as compared with the TBC without any healing particles. Although the mean distance of healing particles from the TC/BC interface does not seem to contribute towards the variance in TBC lifetime, it does potentially affect the damage growth characteristics. Figure 4.6 compares two cases: one in which the mean distance value is near the lower end of its considered range and the other in which it is towards the higher end. Two representative samples from the simulation sample space have been considered for each of the two cases.

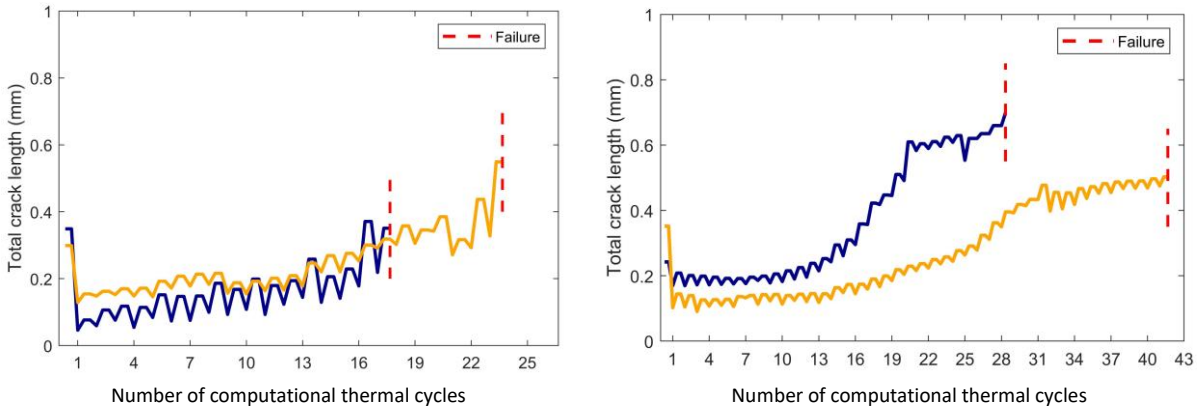

(a) Mean distance ≈ 50 µm (b) Mean distance ≈ 75 µm

Figure 4.6: Comparison of crack growth behaviour for different values of particle mean distance

It can be observed from Figure 4.6(a) that for a lower value of mean distance, the rate of crack growth after the first cycle is fairly constant until catastrophic failure occurs. On the other hand, Figure 4.6(b) indicates that for a higher value of mean distance, the crack growth rate initially increases and stabilizes towards the end until the final failure occurs. This could be attributed to the increased number of available healing sites near the TC/BC interface in case (a), resulting in steady crack growth, whereas a reduced number of healing sites near the TC/BC interface in case (b), resulting in an increasing initial crack growth rate until the total crack length is large enough to encounter multiple healing sites which stabilizes the rate of crack growth.

4.6. COMPARISON WITH THE BENCHMARK TBC

In order to estimate how the use of self-healing particles in TBCs affects the expected lifetime and the underlying scatter as compared with the case of the conventional TBC without any healing particles, a second PCE based surrogate model is developed with the same procedure as described in Figure 3.5. This surrogate model considers the TC/BC interface amplitude and TGO growth rate as the input uncertain variables which are defined over the same respective distributions as that in the surrogate model developed for the self-healing TBC. Equation 4.9 describes the surrogate model developed for the benchmark case.

$$\check{Y}_{benchmark} = 215.42 - 77.40x_2 + 11.65{x_2}^2 - 7.94x_1 + 0.61x_1x_2 + 0.11{x_1}^2 \quad \ldots (4.9)$$

In the above equation, $\check{Y}_{benchmark}$ represents the lifetime of the benchmark TBC in number of computational thermal cycles. The input variables and their respective distributions have been summarized as follows:

x_1	=	TC/BC interface amplitude	Uniform ~ [15,25] µm
x_2	=	TGO growth coefficient	Uniform ~ [2.5,3]

In order to evaluate the surrogate model's goodness of fit and its predictive performance, the adjusted coefficient of determination and leave-one-out cross validation error are calculated:

$$R^2_{adjusted} = 0.99$$

$$Err_{LOO} = 0.91$$

Equation 4.9 has been utilized to acquire the distribution of lifetime for the benchmark TBC. Figure 4.7 compares the box plots which are generated using the lifetime realizations of the surrogate models generated for the benchmark TBC and the self-healing TBC.

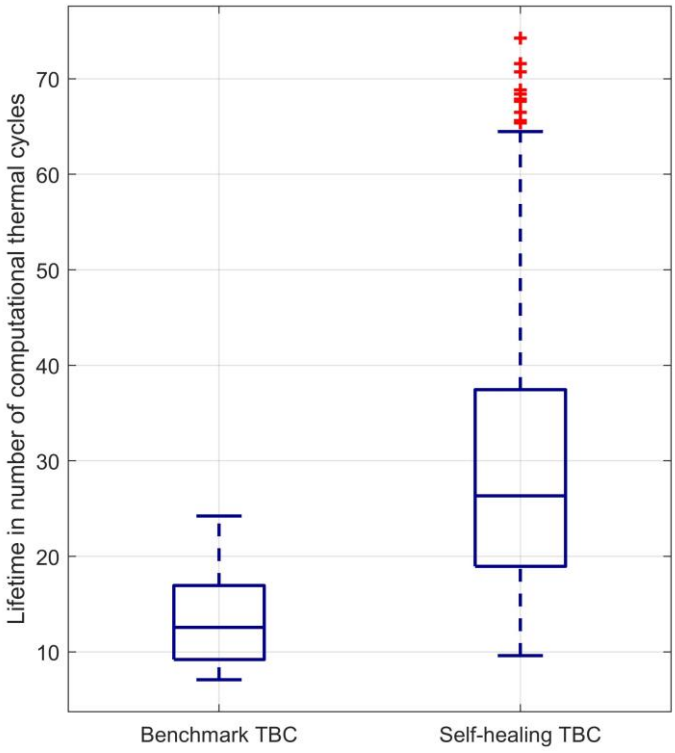

Figure 4.7: Box plot comparison of the lifetime realizations of two surrogate models

It has been found that the surrogate model for the benchmark case provides a mean lifetime value of 13 computational thermal cycles while describing a coefficient of variation (COV) of 35 %. On the other hand, the surrogate model for the self-healing TBC depicts a mean lifetime value of 29 computational thermal cycles and a COV = 45 %. This indicates that for the considered range of values of the input variables, the use of self-healing particles helps to improve the expected TBC lifetime value but at the same time leads to increased scatter in the thermal fatigue life as compared with the benchmark TBC without any healing particles. This observation regarding the increased scatter in lifetime could potentially be attributed to the random distribution and inherent variations in the individual positions of the healing sites within the self-healing TBC. Additionally, the coupled effects of the considered input variables might affect the TBC lifetime, thus contributing to the scatter.

5

CONCLUSION AND RECOMMENDATIONS

Surrogate modelling techniques provide an efficient way of approximating complex and deterministic numerical frameworks. These models are able to take into account the uncertainties in the input variables that are used to design the underlying framework in order to deliver reliable and computationally inexpensive results.

In this thesis, a surrogate model based on polynomial chaos expansion (PCE) has been developed in order to predict the fatigue lifetime of self-healing thermal barrier coatings (TBCs) exposed to thermal cycling. A two-dimensional TBC micromechanical model is considered in which the response to thermal cyclic effects has been described with the help of a cohesive-zone based crack healing model (Ponnusami et al. [89]). TBC design variables such as the top coat (TC)/bond coat (BC) interface amplitude value, growth rate of thermally grown oxide (TGO) layer, diameter and volume fraction of healing particles as well as the mean distance of healing particles from the TC/BC interface have been considered along with their respective uncertainties as inputs for the PCE model.

Latin hypercube sampling has been utilized to derive the experimental design from the input variable distribution space. Finite element simulations have been carried out in ABAQUS on the basis of the design points. These simulations are post-processed in order to obtain self-healing TBC lifetimes which are then utilized to train a second order PCE surrogate model. This model has been compared with a corresponding first order PCE model which demonstrates the better fitting characteristics of the second order PCE. The predictive performance of the two models has been compared using the leave-one-out cross validation approach, the results of which also favour the second order PCE model.

The trained surrogate model is then utilized to obtain the relative contribution of the considered input variables to the variance in the TBC lifetime or the sensitivity indices. It has been found that the TC/BC interface amplitude is the most significant contributor towards the output variance, which is followed by the TGO growth rate. This implies that relatively small changes in the value of the interface amplitude will result in large deviations in the TBC lifetime. As a result, this calls for special efforts to determine the TC/BC interface amplitude value. On the other hand, the variables associated with healing particles have been found to demonstrate relatively minor influence towards the variation in TBC lifetime.

For better visualization of output variation with changes in input variables, TBC lifetime has been plotted as a function of each of the input design variables while the uncertainties in the rest of the variables is propagated through the surrogate model. These uncertainty propagation plots indicate that the expected TBC lifetime reduces with an increase in the TC/BC interface amplitude and TGO growth rate values. Therefore, in order to increase the TBC lifetime, regulation should be exercised during the manufacturing of self-healing TBCs in the form of a control of the powder size and bond coat processing techniques. Even though the mean distance of healing particles from the TC/BC interface makes a negligible contribution towards the TBC lifetime variation, it does seem to positively affect the damage growth characteristics with progression of thermal cycles.

Another second ordered PCE based model has been developed as a surrogate to the TBC micromechanical model without healing particles. A comparison of the lifetime realizations generated by the two surrogate models indicates that the incorporation of healing particles helps in improving the expected value of the TBC lifetime. However, it also leads to an increased amount of scatter in the thermal fatigue life as compared with that of the benchmark or the TBC model without any healing particles.

In sum, the research carried out in this thesis demonstrates the benefit of implementing a surrogate model for developing robust designs for TBCs. The research findings point towards the necessity of an additional layer of analysis over the conventional deterministic approaches in order to estimate the reliability of the results and hence draw informed conclusions. Furthermore, it also paves the way for exploration of other input variables which could possess uncertainness in their values. For example, in this project the material properties have been considered to be constant. However, an uncertainty in the material properties might affect the stress redistribution and growth of damage within the TBC and hence affect the thermal fatigue lifetime. As a result, this provides a scope for uncertainty quantification and sensitivity analysis by considering material properties as input variables for PCE. Since there are no specific guidelines for choosing the order of PCE other than the practical limitations of computational resources, there are possibilities to investigate the surrogate model performance for higher orders.

Nonetheless, as can be observed from Table 3.3, increasing the PCE order leads to an increased number of PCE coefficients and hence a larger experimental design sample space. In such a scenario, sparse polynomial chaos expansions could be explored which facilitate the detection of significant PCE coefficients [108]. As a result, the number of required sample points is reduced. This reduced number of finite element simulations can also promote the development and utilization of a three-dimensional TBC micromechanical model as a black box for uncertainty quantification using surrogate modelling.

APPENDIX-A

ANALYSIS OF COMPUTATIONAL DURATIONS

A considerable number of runs of the finite element model is required to obtain the data points for training the surrogate model. It is known from Section 3.2.3 that the considered order of PCE and the number of input variables lead to a total of 42 sample points. As a result, 42 simulations have to be run in order to obtain the corresponding TBC lifetimes. Since carrying out a finite element simulation is computationally expensive, it becomes necessary to efficiently utilize the available resources.

In order to reduce the total run time, ABAQUS provides the alternative of parallel execution of simulations and analyses. This can be achieved by utilizing multiple processors for solving the task at hand. For instance, the total number of elements within the finite element model will be evenly distributed and assigned to each of the processors which will then perform the operations in parallel. This helps in reducing the total execution time. However, since the divided elements belong to different domains within the model which may share common boundaries, it is necessary to ensure communication between these domains in order to pass information.

Also, computational efforts are required to combine the results obtained by running the task in parallel. As a result, the total execution time consists of the computation time as well as the time required for communication between processors [103]. Therefore, an optimum number of processors needs to be determined to ensure efficient numerical computation. Figure A.1 provides a summary of computational times as a function of number of processors (n_p) used to perform finite element simulations on a particular self-healing TBC sample.

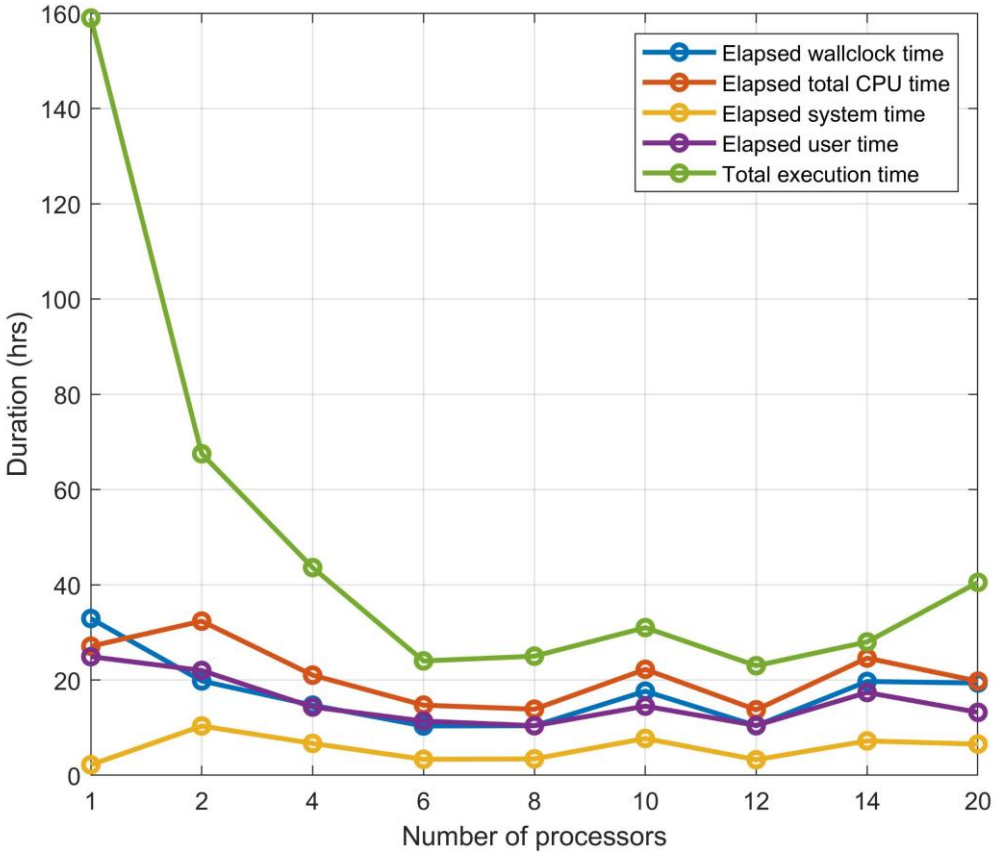

Figure A.1: Summary of computational durations

Here, the elapsed time is representative of the sum of times taken by all the increments in the simulation until failure of the TBC. The wallclock time indicates the actual time taken by the code to run during each increment as measured by a stopwatch. The total CPU time is the sum of the user time or the amount of time taken by the processor to run the desired code and system time which is the time taken by the processor to work on the code-related functions or additional system calls. In addition to these durations, the total execution time consists of the time taken to write and update the ABAQUS model and state files which can be utilized for restarting an analysis as well as the time taken for performing convergence checks for equilibrium after every increment. Figure A.1 indicates that while adhering to computational constraints, the number of simultaneously running simulations can be optimized for reducing the overall time taken for completing 42 simulations. For example, the total execution time for $n_p = 12$ is only slightly lesser than that for $n_p = 6$. This means that instead of running one job with $n_p = 12$, two jobs can be run simultaneously with $n_p = 6$. Additionally, by taking into consideration the amount of data generated for each simulation and the constraints on the available computational memory, it has been found that $n_p = 6$ provides the most efficient recourse for the parallel execution of simulations.

REFERENCES

1. Thakare, J. G., Pandey, C., Mahapatra, M. M., Mulik, R. S. (2020). Thermal Barrier Coatings—A State of the Art Review. *Metals and Materials International*. https://doi.org/10.1007/s12540-020-00705-w.
2. Lashmi, P., Ananthapadmanabhan, P., Unnikrishnan, G., & Aruna, S. (2020). Present status and future prospects of plasma sprayed multilayered thermal barrier coating systems. *Journal of the European Ceramic Society, 40*(8), 2731-2745. https://doi.org/10.1016/j.jeurceramsoc.2020.03.016
3. Cao, X., Vassen, R., & Stoever, D. (2004). Ceramic materials for thermal barrier coatings. *Journal of the European Ceramic Society, 24*(1), 1-10. https://doi.org/10.1016/S0955-2219(03)00129-8.
4. Toscano, J., Vaβen, R., Gil, A., Subanovic, M., Naumenko, D., Singheiser, L., & Quadakkers, W. (2006). Parameters affecting TGO growth and adherence on MCrAlY-bond coats for TBC's. *Surface and Coatings Technology, 201*(7), 3906-3910. https://doi.org/10.1016/j.surfcoat.2006.07.247.
5. Vanevery, K., Krane, M. J., Trice, R. W., Wang, H., Porter, W., Besser, M., . . . Almer, J. (2011). Column Formation in Suspension Plasma-Sprayed Coatings and Resultant Thermal Properties. *Journal of Thermal Spray Technology, 20*(4), 817-828. https://doi.org/10.1007/s11666-011-9632-2.
6. Renteria, A. F., Saruhan, B., Schulz, U., Raetzer-Scheibe, H., Haug, J., & Wiedenmann, A. (2006). Effect of morphology on thermal conductivity of EB-PVD PYSZ TBCs. *Surface and Coatings Technology, 201*(6), 2611-2620. https://doi.org/10.1016/j.surfcoat.2006.05.003
7. T.S. Hille. (2009) Lifetime Modeling of Thermal Barrier Coatings. PhD thesis, TU Delft. http://resolver.tudelft.nl/uuid:1315d027-75d2-4355-9e5e-c60a61e255e3
8. Mehboob, G., Liu, M., Xu, T., Hussain, S., Mehboob, G., & Tahir, A. (2020). A review on failure mechanism of thermal barrier coatings and strategies to extend their lifetime. *Ceramics International, 46*(7), 8497-8521. https://doi.org/10.1016/j.ceramint.2019.12.200
9. Arif, A., Al-Athel, K., & Mostaghimi, J. (2017). Residual Stresses in Thermal Spray Coating. *Comprehensive Materials Finishing,* 56-70. https://doi.org/10.1016/B978-0-12-803581-8.09199-2
10. Zhang, W., Li, G., Zhang, Q., & Yang, G. (2017). Comprehensive damage evaluation of localized spallation of thermal barrier coatings. *Journal of Advanced Ceramics, 6*(3), 230-239. https://doi.org/10.1007/s40145-017-0234-4
11. Krämer, S., Faulhaber, S., Chambers, M., Clarke, D., Levi, C., Hutchinson, J., & Evans, A. (2008). Mechanisms of cracking and delamination within thick thermal barrier systems in aero-engines subject to calcium-magnesium-alumino-silicate (CMAS) penetration. *Materials Science and Engineering: A, 490*(1-2), 26-35. https://doi.org/10.1016/j.msea.2008.01.006
12. Carabat, A., Meijerink, M., Brouwer, J., Kelder, E., Van Ommen, J., van der Zwaag, S., & Sloof, W. (2018). Protecting the $MoSi_2$ healing particles for thermal barrier coatings using a sol-gel produced Al_2O_3 coating. *Journal of the European Ceramic Society, 38*(7), 2728-2734. https://doi.org/10.1016/j.jeurceramsoc.2018.02.002

13. Chen, Y., Zhang, X., van der Zwaag, S., Sloof, W. G., & Xiao, P. (2019). Damage evolution in a self-healing air plasma sprayed thermal barrier coating containing self-shielding $MoSi_2$ particles. *Journal of the American Ceramic Society, 102*(8), 4899-4910. https://doi.org/10.1111/jace.16313
14. Krishnasamy, J., Ponnusami, S. A., Turteltaub, S., & van der Zwaag, S. (2021). Thermal cyclic behavior and lifetime prediction of self-healing thermal barrier coatings. *International Journal of Solids and Structures, 222-223*, 111034. https://doi.org/10.1016/j.ijsolstr.2021.03.021
15. Jayaprakash Krishnasamy. (2020) Computational Analysis of Fracture and Healing in Thermal Barrier Coatings, PhD thesis, TU Delft. https://doi.org/10.4233/uuid:aecd0ff6-e2d8-48f2-9320-c2145f81697c
16. Jeon, S., Jung, S., & Jung, Y. (2017). Effects of Healing Agent on Crack Propagation Behavior in Thermal Barrier Coatings. *Journal of the Korean Ceramic Society, 54*(6), 492-498. https://doi.org/10.4191/kcers.2017.54.6.02
17. Krishnasamy, J., Ponnusami, S. A., Turteltaub, S., & van der Zwaag, S. (2019). Numerical Investigation into the Effect of Splats and Pores on the Thermal Fracture of Air Plasma-Sprayed Thermal Barrier Coatings. *Journal of Thermal Spray Technology, 28*(8), 1881-1892. https://doi.org/10.1007/s11666-019-00949-y
18. Krishnasamy, J., Ponnusami, S. A., Turteltaub, S., & van der Zwaag, S. (2019). Computational investigation of porosity effects on fracture behavior of thermal barrier coatings. *Ceramics International, 45*(16), 20518-20527. https://doi.org/10.1016/j.ceramint.2019.07.031
19. Krishnasamy, J., Ponnusami, S. A., Turteltaub, S., & van der Zwaag, S. (2018). Modelling the fracture behaviour of thermal barrier coatings containing healing particles. *Materials & Design, 157*, 75-86. https://doi.org/10.1016/j.matdes.2018.07.026
20. Jiang, J., Xu, B., Wang, W., Adjei, R. A., Zhao, X., & Liu, Y. (2016). Finite Element Analysis of the Effects of Thermally Grown Oxide Thickness and Interface Asperity on the Cracking Behavior Between the Thermally Grown Oxide and the Bond Coat. *Journal of Engineering for Gas Turbines and Power, 139*(2). https://doi.org/10.1115/1.4034259
21. Ponnusami, S. A., Turteltaub, S., & van der Zwaag, S. (2015). Cohesive-zone modelling of crack nucleation and propagation in particulate composites. *Engineering Fracture Mechanics, 149*, 170-190. https://doi.org/10.1016/j.engfracmech.2015.09.050
22. Leo, C. V., Luk-Cyr, J., Liu, H., Loeffel, K., Al-Athel, K., & Anand, L. (2014). A new methodology for characterizing traction-separation relations for interfacial delamination of thermal barrier coatings. *Acta Materialia, 71*, 306-318. https://doi.org/10.1016/j.actamat.2014.02.034
23. Zhu, W., Yang, L., Guo, J., Zhou, Y., & Lu, C. (2014). Numerical study on interaction of surface cracking and interfacial delamination in thermal barrier coatings under tension. *Applied Surface Science, 315*, 292-298. https://doi.org/10.1016/j.apsusc.2014.07.142
24. Bhatnagar, H., Ghosh, S., & Walter, M. E. (2010). A parametric study of damage initiation and propagation in EB-PVD thermal barrier coatings. *Mechanics of Materials, 42*(1), 96-107. https://doi.org/10.1016/j.mechmat.2009.09.004
25. Rangaraj, S., & Kokini, K. (2004). A Study of Thermal Fracture in Functionally Graded Thermal Barrier Coatings Using a Cohesive Zone Model. *Journal of Engineering Materials and Technology, 126*(1), 103-115. https://doi.org/10.1115/1.1631028

26. Zhang, L., Wang, Y., Fan, W., Gao, Y., Sun, Y., & Bai, Y. (2020). A Simulation Study on the Crack Propagation Behavior of Nanostructured Thermal Barrier Coatings with Tailored Microstructure. *Coatings, 10*(8), 722. https://doi.org/10.3390/coatings10080722
27. Bostancı, S. M., Gürses, E., & Çöker, D. (2019). Finite Element Modelling of TBC Failure Mechanisms by Using XFEM and CZM. *Procedia Structural Integrity, 21*, 91-100. https://doi.org/10.1016/j.prostr.2019.12.090
28. Song, J., Li, S., Yang, X., Shi, D., & Qi, H. (2019). Numerical study on the competitive cracking behavior in TC and interface for thermal barrier coatings under thermal cycle fatigue loading. *Surface and Coatings Technology, 358*, 850-857. https://doi.org/10.1016/j.surfcoat.2018.11.006
29. Jiang, J., Wang, W., Zhao, X., Liu, Y., Cao, Z., & Xiao, P. (2018). Numerical analyses of the residual stress and top coat cracking behavior in thermal barrier coatings under cyclic thermal loading. *Engineering Fracture Mechanics, 196*, 191-205. https://doi.org/10.1016/j.engfracmech.2018.04.031
30. Bai, Y., Wang, Y. H., Wang, Z., Fu, Q. Q., & Han, Z. H. (2014). Influence of unmelted nanoparticles on properties of YSZ nano-coatings. *Surface Engineering, 30*(8), 568-572. https://doi.org/10.1179/1743294414Y.0000000285
31. Zhang, W., Fan, X., & Wang, T. (2011). The surface cracking behavior in air plasma sprayed thermal barrier coating system incorporating interface roughness effect. *Applied Surface* Science, 258(2), 811-817. https://doi.org/10.1016/j.apsusc.2011.08.103
32. Hille, T. S., Nijdam, T. J., Suiker, A. S. J., Turteltaub, S., & Sloof, W. G. (2009). Damage growth triggered by interface irregularities in thermal barrier coatings. *Acta Materialia, 57*(9), 2624–2630. https://doi.org/10.1016/j.actamat.2009.01.022
33. Wang, L., Wei, Z., Cheng, B., Liu, M., Li, G., Dong, H., & Yang, G. (2020). Gradient stiffening induced interfacial cracking and strain tolerant design in thermal barrier coatings. *Ceramics International, 46*(2), 2355-2364. https://doi.org/10.1016/j.ceramint.2019.09.226
34. Wei, Z., & Cai, H. (2020). Comprehensive effects of TGO growth on the stress characteristic and delamination mechanism in lamellar structured thermal barrier coatings. *Ceramics International, 46*(2), 2220-2237. https://doi.org/10.1016/j.ceramint.2019.09.207
35. Fan, X., Xu, R., & Wang, T. (2014). Interfacial delamination of double-ceramic-layer thermal barrier coating system. *Ceramics International, 40*(9), 13793-13802. https://doi.org/10.1016/j.ceramint.2014.05.095
36. Wang, L., Li, D., Yang, J., Shao, F., Zhong, X., Zhao, H., . . . Wang, Y. (2016). Modeling of thermal properties and failure of thermal barrier coatings with the use of finite element methods: A review. *Journal of the European Ceramic Society, 36*(6), 1313-1331. https://doi.org/10.1016/j.jeurceramsoc.2015.12.038
37. Sneha Murali. (2017). Micromechanical modelling of fracture behaviour in self-healing thermal barrier coatings. Master's thesis, TU Delft. http://resolver.tudelft.nl/uuid:eaa0262e-1fb6-4439-b40d-9840f04e9131
38. Le Gratiet, L., Marelli, S., & Sudret, B. (2017). Metamodel-Based sensitivity Analysis: Polynomial Chaos expansions and Gaussian processes. *Handbook of Uncertainty Quantification,* 1289-1325. https://doi.org/10.1007/978-3-319-12385-1_38

39. Han, Z., Lu, W., & Lin, J. (2020). Uncertainty analysis for precipitation and sea-level rise of a variable-density groundwater simulation model based on surrogate models. *Environmental Science and Pollution Research, 27*(22), 28077-28090. https://doi.org/10.1007/s11356-020-09177-2
40. Yin, J., & Tsai, F. T. (2020). Bayesian set pair analysis and machine learning based ensemble surrogates for optimal multi-aquifer system remediation design. *Journal of Hydrology, 580*, 124280. https://doi.org/10.1016/j.jhydrol.2019.124280
41. Marques, A. E., Prates, P. A., Pereira, A. F., Oliveira, M. C., Fernandes, J. V., & Ribeiro, B. M. (2020). Performance comparison of parametric and Non-Parametric regression models for Uncertainty analysis of sheet Metal Forming Processes. *Metals, 10*(4), 457. https://doi.org/10.3390/met10040457
42. Wang, H., Ye, F., Chen, L., & Li, E. (2016). Sheet metal forming optimization by using surrogate modeling techniques. *Chinese Journal of Mechanical Engineering, 30*(1), 22-36. https://doi.org/10.3901/CJME.2016.1020.123
43. Xia, L., Yuan, S., Zou, Z., & Zou, L. (2020). Uncertainty quantification of hydrodynamic forces on the DTC model in shallow water waves using CFD and non-intrusive Polynomial chaos method. *Ocean Engineering, 198*, 106920. https://doi.org/10.1016/j.oceaneng.2020.106920
44. Enderle, B., Rauch, B., Grimm, F., Eckel, G., & Aigner, M. (2020). Non-intrusive uncertainty quantification in the simulation of turbulent Spray combustion using Polynomial chaos Expansion: A case study. *Combustion and Flame, 213*, 26-38. https://doi.org/10.1016/j.combustflame.2019.11.021
45. Hamdia, K. M., Silani, M., Zhuang, X., He, P., & Rabczuk, T. (2017). Stochastic analysis of the fracture toughness of polymeric nanoparticle composites using polynomial chaos expansions. *International Journal of Fracture, 206*(2), 215-227. https://doi.org/10.1007/s10704-017-0210-6
46. Kumar, D., Koutsawa, Y., Rauchs, G., Marchi, M., Kavka, C., & Belouettar, S. (2020). Efficient uncertainty quantification and management in the early stage design of composite applications. *Composite Structures, 251*, 112538. https://doi.org/10.1016/j.compstruct.2020.112538
47. Lopez, R. H., & Silva, C. R. (2015). A non-intrusive methodology for the representation of crack growth stochastic processes. *Mechanics Research Communications, 64*, 23-28. https://doi.org/10.1016/j.mechrescom.2014.12.005
48. Beck, A. T., & Gomes, W. J. (2013). Stochastic fracture mechanics using polynomial chaos. *Probabilistic Engineering Mechanics, 34*, 26-39. https://doi.org/10.1016/j.probengmech.2013.04.002
49. Sadd, M. H. (2019). Constitutive relations and formulation of theories incorporating material microstructure. *Continuum Mechanics Modeling of Material Behavior,* 331-379. https://doi.org/10.1016/B978-0-12-811474-2.00009-5
50. Bäker, M., & Seiler, P. (2017). A Guide to Finite Element Simulations of Thermal Barrier Coatings. *Journal of Thermal Spray Technology, 26*(6), 1146-1160. https://doi.org/10.1007/s11666-017-0592-z

51. Caliez, M., Chaboche, J., Feyel, F., & Kruch, S. (2003). Numerical simulation of EBPVD thermal barrier coatings spallation. *Acta Materialia, 51*(4), 1133-1141. https://doi.org/10.1016/S1359-6454(02)00518-9
52. Sun, Y., Zhang, W., Li, J., & Wang, T. J. (2013). Local stress around cap-like portions of anisotropically and nonuniformly grown oxide layer in thermal barrier coating system. *Journal of Materials Science, 48*(17), 5962-5982. https://doi.org/10.1007/s10853-013-7393-7
53. Ponnusami, S. A., Krishnasamy, J., Turteltaub, S., & van der Zwaag, S. (2018). A micromechanical fracture analysis to investigate the effect of healing particles on the overall mechanical response of a self-healing particulate composite. *Fatigue & Fracture of Engineering Materials & Structures, 42*(2), 533-545. https://doi.org/10.1111/ffe.12929
54. Honarmandi, P., & Arróyave, R. (2020). Uncertainty Quantification and Propagation in Computational Materials Science and Simulation-Assisted Materials Design. *Integrating Materials and Manufacturing Innovation, 9*(1), 103-143. https://doi.org/10.1007/s40192-020-00168-2
55. Wiener, N. (1938). The Homogeneous Chaos. *American Journal of Mathematics, 60*(4), 897-936. https://doi.org/10.2307/2371268
56. Cameron, R., & Martin, W. (1947). The Orthogonal Development of Non-Linear Functionals in Series of Fourier-Hermite Functionals. *Annals of Mathematics, 48*(2), second series, 385-392. https://doi.org/10.2307/1969178
57. Xiu, D., & Karniadakis, G. E. (2002). The Wiener-Askey Polynomial Chaos for Stochastic Differential Equations. *SIAM Journal on Scientific Computing, 24*(2), 619-644. https://doi.org/10.1137/S1064827501387826
58. Sudret, B. (2008). Global sensitivity analysis using polynomial chaos expansions. *Reliability Engineering & System Safety, 93*(7), 964–979. https://doi.org/10.1016/j.ress.2007.04.002
59. Yang, S., Xiong, F., & Wang, F. (2017). Polynomial Chaos Expansion for Probabilistic Uncertainty Propagation. *Uncertainty Quantification and Model Calibration*. http://dx.doi.org/10.5772/intechopen.68484
60. Soize, C., & Ghanem, R. (2004). Physical Systems with Random Uncertainties: Chaos Representations with Arbitrary Probability Measure. *SIAM Journal on Scientific Computing, 26*(2), 395-410. https://doi.org/10.1137/S1064827503424505
61. Bhattacharyya, B. (2017). A critical appraisal of design of experiments for uncertainty quantification. *Archives of Computational Methods in Engineering, 25*(3), 727-751. https://doi.org/10.1007/s11831-017-9211-x
62. Dutta, S., & Gandomi, A. H. (2020). Design of experiments for uncertainty quantification based on polynomial chaos expansion metamodels. *Handbook of Probabilistic Models*, 369-381. https://doi.org/10.1016/B978-0-12-816514-0.00015-1
63. Law, A. M. (2014). A tutorial on design of experiments for simulation modeling. *Proceedings of the Winter Simulation Conference 2014*, 66-80. https://doi.org/10.1109/WSC.2014.7019878
64. Sheikholeslami, R., & Razavi, S. (2017). Progressive Latin Hypercube Sampling: An efficient approach for Robust sampling-based analysis of environmental models. *Environmental Modelling & Software, 93,* 109-126. https://doi.org/10.1016/j.envsoft.2017.03.010

65. Sacks, J., Schiller, S. B., & Welch, W. J. (1989). Designs for computer experiments. *Technometrics, 31*(1), 41-47. https://doi.org/10.2307/1270363
66. Choi, S., Grandhi, R. V., Canfield, R. A., & Pettit, C. L. (2004). Polynomial chaos expansion with Latin Hypercube sampling for Estimating Response Variability. *AIAA Journal, 42*(6), 1191-1198. https://doi.org/10.2514/1.2220
67. Hosder, S., Walters, R., & Balch, M. (2007). Efficient sampling for non-intrusive polynomial chaos applications with multiple uncertain input variables. *48th AIAA/ASME/ASCE/AHS/ASC Structures, Structural Dynamics, and Materials Conference*. https://doi.org/10.2514/6.2007-1939
68. Nguyen, T. H., & Chang, K. (2019). Comparison of the Point-Collocation Non-Intrusive Polynomial (NIPC) and Non-intrusive Spectral Projection (NISP) Methods for the $\gamma - R_\theta$ Transition Model. *Applied Sciences, 9*(7), 1407. https://doi.org/10.3390/app9071407
69. Sudret, B., Marelli, S., & Wiart, J. (2017). Surrogate models for uncertainty quantification: An overview. *2017 11th European Conference on Antennas and Propagation (EUCAP).* https://doi.org/10.23919/EuCAP.2017.7928679
70. Chen, L. (2011). Processing, microstructures and properties of thermal barrier coatings (TBCs) by plasma spraying (PS). *Thermal Barrier Coatings*, 132-160. https://doi.org/10.1533/9780857090829.2.132
71. Eriksson, R., Sjöström, S., Brodin, H., Johansson, S., Östergren, L., & Li, X. (2013). TBC bond coat–top coat interface roughness: Influence on fatigue life and modelling aspects. *Surface and Coatings Technology, 236*, 230-238. https://doi.org/10.1016/j.surfcoat.2013.09.051
72. Martins, J. P., Chen, Y., Brewster, G., Mcintyre, R., & Xiao, P. (2020). Investigation of the bond coat interface topography effect on lifetime, microstructure and mechanical properties of air-plasma sprayed thermal barrier coatings. *Journal of the European Ceramic Society, 40*(15), 5719-5730. https://doi.org/10.1016/j.jeurceramsoc.2020.05.082
73. Jiang, J., Xu, B., Wang, W., Adjei, R. A., Zhao, X., & Liu, Y. (2016). Finite Element Analysis of the Effects of Thermally Grown Oxide Thickness and Interface Asperity on the Cracking Behavior Between the Thermally Grown Oxide and the Bond Coat. *Journal of Engineering for Gas Turbines and Power, 139*(2). https://doi.org/10.1115/1.4034259
74. Lim, L., & Meguid, S. (2019). Temperature dependent dynamic growth of thermally grown oxide in thermal barrier coatings. *Materials & Design, 164*, 107543. https://doi.org/10.1016/j.matdes.2018.107543
75. Jiang, J., Wang, W., Zhao, X., Liu, Y., Cao, Z., & Xiao, P. (2018). Numerical analyses of the residual stress and top coat cracking behaviour in thermal barrier coatings under cyclic thermal loading. *Engineering Fracture Mechanics, 196*, 191-205. https://doi.org/10.1016/j.engfracmech.2018.04.031
76. Hille, T., Turteltaub, S., & Suiker, A. (2011). Oxide growth and damage evolution in thermal barrier coatings. *Engineering Fracture Mechanics, 78*(10), 2139-2152. https://doi.org/10.1016/j.engfracmech.2011.04.003
77. Nakajima, R., Katori, H., Ito, K., Arai, M., & Suidzu, T. (2020). Numerical simulation on internal stress evolution based on formation of thermally grown oxide in thermal barrier coatings. *Engineering Research Express, 2*(2), 025037. https://doi.org/10.1088/2631-8695/ab9717

78. Fox, A., & Clyne, T. (2004). Oxygen transport by gas permeation through the zirconia layer in plasma sprayed thermal barrier coatings. *Surface and Coatings Technology, 184*(2-3), 311-321. https://doi.org/10.1016/j.surfcoat.2003.10.018
79. Ogawa, K., & Nakano A. (2013). Thermally grown oxide growth behavior and its impedance properties of thermal barrier coatings with cold sprayed and low pressure plasma sprayed bond coatings. *Journal of the Society of Materials Science, Japan, 62*(2), 131-136. https://doi.org/10.2472/jsms.62.131
80. Nozahic, F., Monceau, D., & Estournès, C. (2016). Thermal cycling and reactivity of a MoSi2/ZrO2 composite designed for self-healing thermal barrier coatings. *Materials & Design, 94*, 444-448. https://doi.org/10.1016/j.matdes.2016.01.054
81. Kulczyk-Malecka, J., Zhang, X., Carr, J., Carabat, A. L., Sloof, W. G., van der Zwaag, S., . . . Xiao, P. (2016). Influence of embedded MoSi2 particles on the high temperature thermal conductivity of SPS produced yttria-stabilised zirconia model thermal barrier coatings. *Surface and Coatings Technology, 308*, 31-39. https://doi.org/10.1016/j.surfcoat.2016.07.113
82. Nozahic, F., Estournès, C., Carabat, A. L., Sloof, W. G., van der Zwaag, S., & Monceau, D. (2018). Self-healing thermal barrier coating systems fabricated by spark plasma sintering. *Materials & Design, 143*, 204-213. https://doi.org/10.1016/j.matdes.2018.02.001
83. Koch, D., Mauer, G., & Vaßen, R. (2017). Manufacturing of Composite Coatings by Atmospheric Plasma Spraying Using Different Feed-Stock Materials as YSZ and MoSi2. *Journal of Thermal Spray Technology, 26*(4), 708-716. https://doi.org/10.1007/s11666-017-0537-6
84. Lv, Z., & Chen, H. (2013). Self-healing efficiency of unhydrated cement nuclei for dome-like crack mode in cementitious materials. *Materials and Structures, 46*(11), 1881-1892. https://doi.org/10.1617/s11527-013-0027-3
85. Jinnestrand, M., & Sjöström, S. (2001). Investigation by 3D FE simulations of delamination crack initiation in TBC caused by alumina growth. *Surface and Coatings Technology, 135*(2-3), 188-195. https://doi.org/10.1016/S0257-8972(00)01084-7
86. Bostancı, S. M., Gürses, E., & Çöker, D. (2019). Finite Element Modelling of TBC Failure Mechanisms by Using XFEM and CZM. *Procedia Structural Integrity, 21*, 91-100. https://doi.org/10.1016/j.prostr.2019.12.090
87. Saucedo-Mora, L., Slámečka, K., Thandavamoorthy, U., & Marrow, T. J. (2015). Multi-scale modeling of damage development in a thermal barrier coating. *Surface and Coatings Technology, 276*, 399–407. https://doi.org/10.1016/j.surfcoat.2015.06.038
88. Geuzaine, C., & Remacle, J.-F. (2009). Gmsh: A 3-D finite element mesh generator with built-in pre- and post-processing facilities. International Journal for Numerical Methods in Engineering, 79(11), 1309–1331. https://doi.org/10.1002/nme.2579
89. Ponnusami, S. A., Krishnasamy, J., Turteltaub, S., & van der Zwaag, S. (2018). A cohesive-zone crack healing model for self-healing materials. *International Journal of Solids and Structures, 134*, 249–263. https://doi.org/10.1016/j.ijsolstr.2017.11.004
90. Wei, Z.-Y., & Cai, H.-N. (2020). Comprehensive effects of TGO growth on the stress characteristic and delamination mechanism in lamellar structured thermal barrier coatings. *Ceramics International, 46*(2), 2220–2237. https://doi.org/10.1016/j.ceramint.2019.09.207

91. Shen, Q., Yang, L., Zhou, Y. C., Wei, Y. G., & Wang, N. G. (2017). Models for predicting TGO growth to rough interface in TBCs. *Surface and Coatings Technology, 325*, 219–228. https://doi.org/10.1016/j.surfcoat.2017.06.001
92. Beck, T., Herzog, R., Trunova, O., Offermann, M., Steinbrech, R. W., & Singheiser, L. (2008). Damage mechanisms and lifetime behavior of plasma-sprayed thermal barrier coating systems for gas turbines — Part II: Modeling. *Surface and Coatings Technology, 202*(24), 5901–5908. https://doi.org/10.1016/j.surfcoat.2008.06.132
93. Smith, M. (2009). *ABAQUS/Standard User's Manual, Version 6.9*. Dassault Systèmes Simulia Corp.
94. Feinberg, J., & Langtangen, H. P. (2015). Chaospy: An open source tool for designing methods of uncertainty quantification. *Journal of Computational Science, 11*, 46–57. https://doi.org/10.1016/j.jocs.2015.08.008
95. Sudret, B. (2007). Uncertainty propagation and sensitivity analysis in mechanical models - Contributions to structural reliability and stochastic spectral methods. Habilitation à Diriger des Recherches. Vol. 147, Clermont-Ferrand, France: Université Blaise Pascal
96. Sudret, B. (2014) Polynomial chaos expansions and stochastic finite element methods, In: Risk and Reliability in Geotechnical Engineering (Chap. 6), K.-K. Phoon & J. Ching (Eds.), CRC Press, 265-300
97. Pedregosa et al. (2011) Scikit-learn: Machine Learning in Python. *Journal of Machine Learning Research, 12*, 2825-2830.
98. Alam, M. S., Sultana, N., & Hossain, S. M. Z. (2021). Bayesian optimization algorithm based support vector regression analysis for estimation of shear capacity of FRP reinforced concrete members. *Applied Soft Computing, 105*, 107281. https://doi.org/10.1016/j.asoc.2021.107281
99. Hu, Q., Huang, Q., Yang, D., & Liu, H. (2021). Prediction of breakthrough curves in a fixed-bed column based on normalized Gudermannian and error functions. *Journal of Molecular Liquids, 323*, 115061. https://doi.org/10.1016/j.molliq.2020.115061
100. Blatman, G., & Sudret, B. (2011). Adaptive sparse polynomial chaos expansion based on least angle regression. *Journal of Computational Physics, 230*(6), 2345–2367. https://doi.org/10.1016/j.jcp.2010.12.021
101. Blatman, G., & Sudret, B. (2010). Efficient computation of global sensitivity indices using sparse polynomial chaos expansions. *Reliability Engineering & System Safety, 95*(11), 1216–1229. https://doi.org/10.1016/j.ress.2010.06.015
102. Weiss, N. A., Holmes, P. T., & Hardy, M. (2006). A course in probability. *Pearson Addison Wesley*, 385-386. ISBN: 9780201774719
103. Alias, N., Islam, Md. Rajibul, Muhamad, Nurul Ain Zhafarina Satam, N., & Hamzah, N. (2010) An improved parallel AGE method to solve incomplete blow-up problem through high performance computing system. *International Journal of Open Problems in Computer Science and Mathematics, 3*(3), 369-389.
104. Busso, E. P., Qian, Z. Q., Taylor, M. P., & Evans, H. E. (2009). The influence of bondcoat and topcoat mechanical properties on stress development in thermal barrier coating systems. *Acta Materialia, 57*(8), 2349–2361. https://doi.org/10.1016/j.actamat.2009.01.017

105. Skalka, P., Slámečka, K., Pokluda, J., & Čelko, L. (2015). Stability of plasma-sprayed thermal barrier coatings: The role of the waviness of the bond coat and the thickness of the thermally grown oxide layer. *Surface and Coatings Technology, 274*, 26–36. https://doi.org/10.1016/j.surfcoat.2015.04.021
106. Bolelli, G., Righi, M. G., Mughal, M. Z., Moscatelli, R., Ligabue, O., Antolotti, N., Sebastiani, M., Lusvarghi, L., & Bemporad, E. (2019). Damage progression in thermal barrier coating systems during thermal cycling: A nano-mechanical assessment. *Materials & Design, 166*, 107615. https://doi.org/10.1016/j.matdes.2019.107615
107. Chen, W., Liu, M., Zhang, J., Deng, Z., & Mao, J. (2018). High-temperature oxidation behavior and analysis of impedance spectroscopy of 7YSZ thermal barrier coating prepared by plasma spray-physical vapor deposition. *Chinese Journal of Aeronautics, 31*(8), 1764–1773. https://doi.org/10.1016/j.cja.2017.12.008
108. Blatman, G., & Sudret, B. (2008). Sparse polynomial chaos expansions and adaptive stochastic finite elements using a regression approach. *Comptes Rendus Mécanique, 336*(6), 518–523. https://doi.org/10.1016/j.crme.2008.02.013
109. Sloof, W.G., & Sondervan, M. (2017) Self-healing thermal barrier coatings, *Publishable final summary*, SAMBA.